National University of Singapore

Honours Project in Physics

Asymptotic Solution to the QCD-parton branching equation

Aren Tang Minyi

Supervisors:

A/Prof Phil Chan Aik Hui

Prof Oh Choo Hiap

A thesis submitted for the degree of:

Bachelor of Science with Honours

2013/2014

Abstract

A study of charged multiplicity data from the Large Hadron Collider was conducted. The study seeks to describe the obtained multiplicity data with a new multiplicity distribution. This new distribution was derived by obtaining the Asymptotic Solution to Giovanninis QCD-parton branching equation. Experimental pp collision data from the CMS experiment at the LHC were fitted with the aforementioned Asymptotic Solution. The charged particle multiplicity data used are at centre-of-momentum energies of $\sqrt{s} = 900$, 2360 and 7000 GeV with pseudorapidity cuts of $\eta_c = 0.5$, 1.0, 1.5, 2.0 and 2.4 (full phase space). The Asymptotic Solution is able to provide a reasonably good fit to the experimental data. Although the Asymptotic Solution was unable to reproduce the shoulder structure seen in the experimental data, the fit in the shoulder region were all well within the range of experimental uncertainties. Analysis of the behaviour of the fit parameters with respect to pseudorapidity intervals η_c and centre-of-momentum energies $\sqrt{s}$ were conducted. The analysis indicates that gluon branching becomes more dominant compared to quark branching as energy increases. Furthermore, the mean multiplicity also increases with increasing $\sqrt{s}$. Additionally, results from the analysis point to KNO scaling violation at high η_c. Finally, a prediction of the multiplicity distributions for energies of 8000, 13000, and 14000 GeV was made. One hopes to conduct a future study with an improved theoretical model which builds on the results obtained from this study. One looks forward to comparing the predictions made in this study to the experimental data when the LHC is fully operational in 2015.

Acknowledgements

This thesis marks the end of my time as an undergraduate student in NUS. As such there is much to give thanks for and many people to acknowledge.

Firstly, I would like to thank God, without whom, the study of physics would be impossible. I thank God for blessing me with sufficient mental faculties to complete this project without losing my sanity.

I would also like to thank my family. They have been there for me and have given both moral and financial support throughout this often stressful tenure in NUS. Without them, I do not think I would have made it this far in my studies; I look forward to providing for them in the future.

Next, I would like to thank my project supervisors Assoc. Prof. Phil Chan and Prof. Oh C.H. for their guidance during the course of the project. Their comments and advice has been invaluable in my understanding of the subject matter whilst their experience in the field has often enabled me a fresh perspective when encountering problems.

A special thank you to my colleagues in the department, namely, John, Jamil, Michel, Theodore, Koon Tong, Melvin, Jacqueline, Kim, Kirsten; and also to others that I do not have the space to name here. Thank you for being the only other people who understand the joys and pains of studying physics in NUS. May our friendships continue on even after we move on from this phase of our lives.

Contents

1 Introduction **1**

1.1 Particle Physics 1
1.2 Phenomenology 2
1.3 Hadronization 3
1.4 Charged Particle Multiplicity 3
1.5 Overview and Outlook 4

2 Asymptotic Solution **5**

2.1 Introduction 5
2.1.1 Partons 5
2.1.2 Jets 5
2.2 Formalism 6
2.3 Derivation 8
2.3.1 Method of Laplace Transform 9
2.3.2 Saddle Point Approximation 13
2.3.3 Relation to the Generalized Multiplicity Distribution . 17
2.4 Mean, Moments, KNO-Scaling 17
2.4.1 KNO-Scaling 18
2.5 Summary 19

3 Data Analysis **20**

3.1 About the Data 20
3.1.1 Primary Interactions 21
3.1.2 Non-Single-Diffractive (NSD) Events 21
3.2 Analysis Methodology 22

3.3 Analysis ($\sqrt{s} = 900$ GeV) 24
3.4 Analysis ($\sqrt{s} = 2360$ GeV) 30
3.5 Analysis ($\sqrt{s} = 7000$ GeV) 35
3.6 Comparison Across Energies 40
3.6.1 Violation of KNO Scaling 46
3.7 Discussion 48

4 Prediction for Higher Energies **49**
4.1 Extrapolation of Fit Parameters 49
4.2 Predictions 50

5 Concluding Remarks **55**
5.1 Conclusions 55
5.2 Future Work 56

A Markov Branching Process **58**

B Commonly Used Variables **59**
B.1 Pseudorapidity, η 59
B.1.1 Definition 59
B.1.2 Relation to Rapidity, y 60
B.1.3 y vs η and their importance 61
B.2 Mandlestam Variables 62
B.2.1 More on $\sqrt{s}$ 63

C Local Parton Hadron Duality **64**

D Feynman and KNO Scaling **65**
D.1 Feynman Scaling 65
D.2 KNO scaling 66

References **67**

List of Figures

2.1 Schematic illustration of a typical event with QCD jets. 6

3.1 Different scattering events. 21
3.2 Multiplicity distribution at 900 GeV for various η_c fitted with the Asymptotic Solution. 24
3.2 *(Cont.)* 25
3.2 *(Cont.)* 26
3.3 Comparison of experimental and theoretical C_q moments for 900 GeV. 29
3.4 Multiplicity distribution at 2360 GeV for various η_c fitted with the Asymptotic Solution. 30
3.4 *(Cont.)* 31
3.4 *(Cont.)* 32
3.5 Comparison of experimental and theoretical C_q moments for 2360 GeV. 34
3.6 Multiplicity distribution at 7000 GeV for various η_c fitted with the Asymptotic Solution. 35
3.6 *(Cont.)* 36
3.6 *(Cont.)* 37
3.7 Comparison of experimental and theoretical C_q moments for 7000 GeV. 39
3.8 Comparison of Fit Parameters Across Different Energies . . . 41
3.8 *(Cont.)* 42
3.8 *(Cont.)* 43
3.9 Comparison of $\overline{n}$ across different energies and η_c. 45

3.10 KNO Plots 46

4.1 Predicted Curves for 8 TeV, 13 TeV and 14 TeV 53
4.2 Predicted KNO Plots 54

B.1 Schematic Illustration for Pseudorapidity 59
B.2 Plot of Pseudorapidity η against polar angle θ. 60
B.3 Feynman Diagrams representing different scattering channels . 62

List of Tables

3.1 Fit Parameters for $\sqrt{s} = 900$ GeV at various η_c. 27
3.2 Mean Multiplicity and C_q moments for $\sqrt{s} = 900$ GeV. 28
3.3 Fit Parameters for $\sqrt{s} = 2360$ GeV at various η_c. 33
3.4 Mean Multiplicity and C_q moments for $\sqrt{s} = 2360$ GeV. . . . 34
3.5 Fit Parameters for $\sqrt{s} = 7000$ GeV at various η_c. 38
3.6 Mean Multiplicity and C_q moments for $\sqrt{s} = 7000$ GeV. . . . 38
3.7 Comparison of α across different energies. 40
3.8 Comparison of β across different energies. 40
3.9 Comparison of D across different energies. 40
3.10 Comparison of k across different energies. 41
3.11 Comparison of k' across different energies. 41

4.1 Predicted Fit Parameters for 8000 GeV 50
4.2 Predicted Mean and C_q moments for 8000 GeV 51
4.3 Predicted Fit Parameters for 13000 GeV 51
4.4 Predicted Mean and C_q moments for 13000 GeV 51
4.5 Predicted Fit Parameters for 14000 GeV 52
4.6 Predicted Mean and C_q moments for 14000 GeV 52

Chapter 1

Introduction

1.1 Particle Physics

The field of particle physics has flourished in recent times, growing in tandem with modern technology, with many new technological advances stemming from the pursuit of experimental results in this field. These experimental results and observations have given shape to our current models of understanding.

One of the milestones of particle physics was the quark theory proposed by Gell-Mann and Zweig in 1964. They postulated that many particles discovered were not elementary, but had an even more basic structure known as "quarks". Experimental evidence in later years would support the notion of quarks.

Our understanding of particle physics was further advanced by the unification of the electromagnetic force and weak force. The so-called electroweak unification was separately proposed by Glashow, Weinberg and Salam. The electroweak theory posits the existence of mediator bosons ($W^{\pm}$ and Z^0 for weak and photons for electromagnetic) which are the interaction carriers in particle interactions. This was the first step to what is currently known as the Standard Model of Particle Physics. The introduction of Quantum Electrodynamics (QED) and subsequently Quantum Chromodynamics (QCD) further spurred the advancement of the field. Gluons act as the mediator

bosons for strong interactions (analog to the photon in QED). Both QED and QCD led to the development of the Standard Model of Particle Physics.

Experiments to search for all the aforementioned particles require the acceleration of elementary particles to very high energies. As such particle accelerators are specially built to study the processes of particle production. As of the time of writing, CERN has become the first to observe a Higgs boson[1], which has given support to the Standard Model. This was done at the Large Hadron Collider (LHC) by both the ATLAS and CMS experiments. In early 2015, the LHC is set to operate at full energy of approximately 14 TeV. With the discovery of the Higgs, the field particle physics has never been more vibrant. Many questions remain unanswered and studies in the field may unlock more secrets of the universe.

1.2 Phenomenology

Phenomenology is an aspect of physics that can be best described as a bridge between the realms of the theoretical that of the experimental. This practice involves describing and relating various empirical phenomena to known fundamental theoretical models.

In particle physics in particular, phenomenology seeks to bring describe experimental data with theoretical models. As such phenomenologists are not only familiar with varying mathematical models, they are required to have a certain degree of imagination and creativity so as to obtain the most suitable models without bias.

The significance of this particular field is noticeable in the research frontier, as phenomenological work is usually the first line of attack for new experimental data. Often, there are no well established theories which are able to satisfactorily explain the obtained experimental data, leading to a phenomenological approach. As more ground-breaking research is conducted in the experimental sector, there is great need for phenomenological work to interpret the large amounts of observations recorded.

1.3 Hadronization

In nature, lone quarks are not detected; they form baryons and mesons which are then detected. This process of forming baryons and mesons is called hadronization. Although the Standard Model does well in explaining many phenomena, it cannot explain the mechanism of hadronization. In fact, till today, the mechanism of hadronization is not well understood[2].

In order to shed some light onto this phenomena, particle physicists turn to study charged particle multiplicity distributions obtained from particle colliders. It is thought that since quarks fragment and hadronize in the form of jets, by studying the particle multiplicity, one takes a step closer to understanding hadronization.

1.4 Charged Particle Multiplicity & Multiplicity Distributions

Particle multiplicity refers to the number of hadrons produced (detected) after each event. This number varies from event to event. Thus one can calculate the probability that a certain number of hadrons are produced. Thus, a probability distribution can be obtained. The probability distribution is known as a multiplicity distribution.

Among the many distributions used to explain the multiplicity distribution are the Negative Binomial Distribution (NBD) and the Generalized Multiplicity Distribution (GMD)[3].

Although the both NBD and GMD can describe the data well at low energies, a single distribution is insufficient in describing the data satisfactorily. The main reason is that at higher energies there seems to be a 'shouldering' in the multiplicity distribution. As such, multiple component NBD and GMD[4,5] fits are used to better model the multiplicity data. Since there is no one 'best' model that can perfectly describe the data, research in this area is still ongoing[4,6–13]. The behaviour of the multiplicity distribution remains one of the unsolved mysteries of particle physics.

1.5 Overview and Outlook

In this study, one seeks to describe the multiplicity data by the asymptotic solution obtained by solving Giovannini's QCD-parton branching equation [14]. The obtained asymptotic solution has the form of another multiplicity distribution. Hence, a single distribution fit (of collider data) will be performed with this solution.

A good description of the data by this asymptotic solution will hopefully shed more light on charged particle multiplicities and thus help in the understanding of the hadronization mechanism.

The next few chapters are dedicated to first deriving the asymptotic solution, the results of the analysis, discussions and finally a conclusion to this study.

Chapter 2

Asymptotic Solution to the QCD-Parton Branching Equation

2.1 Introduction

2.1.1 Partons

The term 'parton' was coined by Richard Feynman himself as the constituent point-like objects inside a hadron. These point like objects are what we know today as quarks and gluons. Partons are coloured objects, hence, we are unable to observe them in Nature. In an interaction, the main signature of parton production are the detection of jets.

2.1.2 Jets

Jets are a result of QCD confinement. Due to colour-neutrality of all observable objects, lone partons cannot exist freely. As a result, these partons will fragment and hadronize into colourless hadrons before they can be detected. The fragmentation and subsequent hadronization of partons will form narrow cones of hadrons close to the direction in which the initial parton was travelling. This spray of collimated hadrons is called a jet.

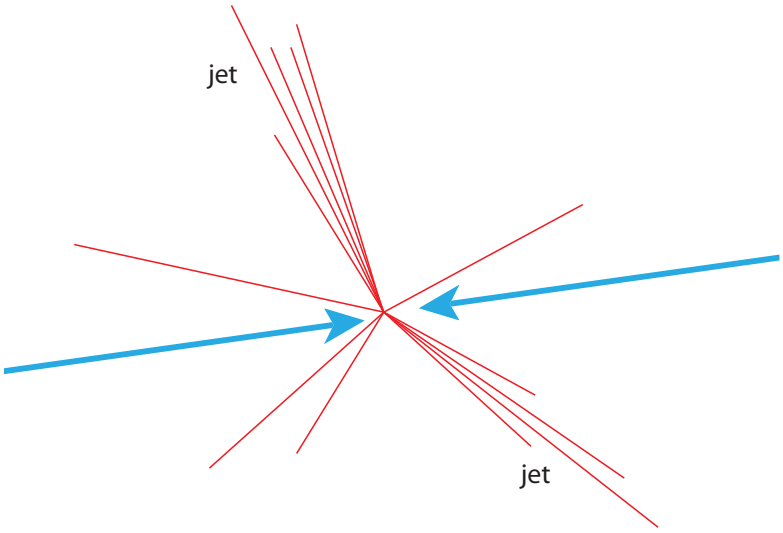

Figure 2.1: Schematic illustration of a typical event with QCD jets.

2.2 Formalism

There are three main fundamental processes that contribute toward the overall quark and gluon distribution QCD jets. Furthermore, since high energy processes are considered, gluon activity also plays a role in the minijet cross section. As such there are a total of four processes that are considered.

i. gluon fission: $g \to g + g$,

ii. quark brehmsstrahlung: $q \to q + g$,

iii. quark pair creation: $g \to q + \bar{q}$,

iv. four gluon vertex: $g \to g + g + g$.

The first three are the main fundamental processes whilst the last process is due to the role of gluon activity.

The four processes contribute with different weights, i.e. they have differing probabilities of occurring. The probabilities of the processes are:

Process	**Probability**
$g \to g + g$	A
$q \to q + g$	$\tilde{A}$
$g \to q + \bar{q}$	B
$g \to g + g + g$	C

Let t be the natural evolution parameter in QCD where

$$t = \frac{6}{11N_c - 2N_f} \ln \left[\frac{\ln(Q^2/\mu^2)}{\ln(Q_0^2/\mu^2)} \right], \tag{2.1}$$

and

$$\begin{aligned} Q &= \text{the initial parton invariant mass} \\ Q_0 &= \text{the hadronization mass} \\ \mu &= \text{a few GeV (a QCD mass scale)} \\ N_c &= \text{number of colors} \\ N_f &= \text{number of flavors} \end{aligned}$$

Giovannini proposed that this evolution of parton jets can be intepreted as a **Markov branching process**[14].

Consider $A\Delta t$ as the probability that gluon will, infinitesimal interval Δt, convert into two gluons (gluon fission occurs). Similarly the probabilities of quark brehmsstrahlung, quark pair-creation and the formation of a four gluon vertex is given by $\tilde{A}\Delta t$, $B\Delta t$ and $C\Delta t$ respectively. Thus, one arrives at the following Markov equation:

$$\begin{aligned} P_{m,n}(t + \Delta t) = (1 - An\Delta t - \tilde{A}m\Delta t - Bn\Delta t - Cn\Delta t) \times P_{m,n}(t) \\ + A(n-1)\Delta t P_{m,n-1}(t) \\ + \tilde{A}m\Delta t P_{m,n-1}(t) \\ + B(n+1)\Delta t P_{m-2,n+1}(t) \\ + C(n-2)\Delta t P_{m,n-2}(t) \end{aligned} \tag{2.2}$$

This branching process of partons terminates at Q_0, after producing m quarks and n gluons, and is expected to hadronize.

As $\Delta t \to 0$ the Giovannini QCD-parton branching equation is obtained:

$$\begin{aligned}\frac{\mathrm{d}P}{\mathrm{d}t} = & -AnP_n + A(n-1)P_{n-1} \\ & -\tilde{A}mP_n + \tilde{A}mP_{n-1} \\ & -BnP_n + B(n+1)P_{n+1} \\ & -CnP_n + C(n-2)P_{n-2}\end{aligned} \tag{2.3}$$

Since one is dealing with data from the Large Hadron Collider, the large energy limit (TeV range) is considered. Thus, $A, \tilde{A} \geq B \geq C$, and the quark evolution is neglected. An initial condition of

$$P_n(t=0) = \delta_{n,k'} \tag{2.4}$$

is imposed, i.e., **initially after collisions there are k' gluons formed**. An asymptotic solution to Eqn. (2.3) has been obtained.[15]

2.3 Derivation of the Asymptotic Solution

A solution of the Giovannini QCD-parton branching equation (2.3) is first obtained by looking for a continuous-variable approximation. Here, one approximates n as a continuous variable x. $P_n(t)$ is replaced by $P(x,t)$ and λn by λx where $\lambda = A, A^\dagger, B, C$ and $A^\dagger = m\tilde{A}$.

Thus, Eqn. (2.3) can be rewritten as:

$$\begin{aligned}\frac{\partial P(x,t)}{\partial t} = & -AxP(x,t) + A(x-1)P(x-1,t) \\ & -A^\dagger P(x,t) + A^\dagger P(x-1,t) \\ & -BxP(x,t) + B(x+1)P(x+1,t) \\ & -CxP(x,t) + C(x-2)P(x-2,t)\end{aligned} \tag{2.5}$$

The solution to this partial differential equation is obtained using two techniques. The first is the method of Laplace transform and the second is that of the method of steepest descent (or saddle point approximation).

2.3.1 Method of Laplace Transform

First recall the definition of the Laplace Transform and its inverse:

$$P^*(x,s) = \int_0^\infty e^{-st} P(x,t)\,\mathrm{d}t, \qquad \text{Real (s)} > 0 \tag{2.6a}$$

$$P(x,t) = \frac{1}{2\pi i}\int_{C-i\infty}^{C+i\infty} e^{st} P^*(x,s)\,\mathrm{d}s \tag{2.6b}$$

where C is positive and greater than the real parts of all singularities of $P^*(x,s)$.

Also note that:

$$\left[\frac{\partial P(x,t)}{\partial t}\right]^* = -P(x,t=0) + sP^*(x,s) \tag{2.6c}$$

Starting with initial conditions $P(x=k',t=0)=1$, the Laplace transform is applied on both sides of Eqn. (2.5):

$$\begin{aligned}\left(\frac{\partial P}{\partial t}\right)^* = &-AxP^*(x,s) + A(x-1)P^*(x-1,s)\\ &-A^\dagger P^*(x,s) + A^\dagger P^*(x-1,s)\\ &-BxP^*(x,s) + B(x+1)P^*(x+1,s)\\ &-CxP^*(x,s) + C(x-2)P^*(x-2,s)\end{aligned} \tag{2.7}$$

Firstly, consider when $x > k'$:

$$-P(x,t=0) + sP^*(x,s) = \text{RHS of Eqn. (2.7)} \tag{2.8}$$

Since $P(x>k',t=0)=0$ for $x \neq k'$ (due to the initial conditions), the

above equation reduces to:

$$sP^*(x,s) = \text{RHS of Eqn. (2.7)} \tag{2.9}$$

Now, consider when $x = k'$:

$$-P(x = k', t = 0) + sP^*(x,s) = -[Ax + A^\dagger + Bx + Cx]P^*(x,s) \tag{2.10}$$

Recalling Eqn. (2.4) one arrives at:

$$P^*(x = k', s) = \frac{1}{s + A^\dagger + (A + B + C)k'} \tag{2.11}$$

Eqn. (2.9) is now considered. Let $L(x,s) = \ln P^*(x,s)$. For simplicity, all $L(x,s)$ will be written as $L(x)$. Eqn. (2.9) will become:

$$\begin{aligned} se^{L(x)} = & -Axe^{L(x)} + A(x-1)e^{L(x-1)} \\ & - A^\dagger e^{L(x)} + A^\dagger e^{L(x-1)} \\ & - Bxe^{L(x)} + B(x+1)e^{L(x+1)} \\ & - Cxe^{L(x)} + C(x-2)e^{L(x-2)} \end{aligned} \tag{2.12}$$

Suppose, $L(x+1) \sim L(x)$ and $L(x-2) \sim L(x-1)$ due to the large number of gluons created in high energy collisions. Then, Eqn. (2.12) can be cast in the following form:

$$\begin{aligned} se^{L(x)} = & -[Ax + A^\dagger + Bx + Cx]e^{L(x)} \\ & + [A(x-1) + A^\dagger + C(x-2)]e^{L(x-1)} \\ & + B(x+1)e^{L(x)} \end{aligned} \tag{2.13}$$

Since x is a continuous variable, $L(x-1)$ can be expanded about $L(x)$

by a Taylor series up to the first differential coefficient.

$$\begin{aligned} L(x-1) &= L(x) + (-1)\frac{\partial L(x)}{\partial x} \\ &= L(x) - L'(x) \end{aligned} \tag{2.14}$$

where $L'(x) = \frac{\partial L(x)}{\partial x}$.

From (2.14) we have

$$e^{L(x-1)} = e^{L(x)} e^{-L'(x)} \tag{2.15}$$

Substituting (2.15) into (2.13) and performing simple algebraic manipulations, one obtains:

$$-\frac{\partial L(x)}{\partial x} = \ln \frac{s + [A^\dagger - B + (A+C)x]}{(A+C)x + A^\dagger - A - 2C} \tag{2.16}$$

Making these four substitutions

$$\alpha = A^\dagger - B \tag{2.17a}$$

$$\beta = A + C \tag{2.17b}$$

$$\gamma = A^\dagger - A - 2C \tag{2.17c}$$

$$D = A + B + C \tag{2.17d}$$

one arrives at:

$$-\frac{\partial L(x)}{\partial x} = \ln \frac{s + \alpha + \beta x}{\gamma + \beta x} \tag{2.18}$$

Integrating (2.18) to give a first approximation. One obtains:

$$L_1(x, s) = -\int_x^{k'} \ln \frac{s + \alpha + \beta\omega}{\gamma + \beta\omega} \, \mathrm{d}\omega - \ln [s + A^\dagger + Dk'] \tag{2.19}$$

where $L(k', s) = \ln P^*(x = k', s)$ can be obtained from (2.11).

A more accurate solution can be obtained if one considers the second

derivatives as well. Eqn. (2.14) becomes:

$$L(x-1) = L(x) - L'(x) + \frac{1}{2}L''(x) \tag{2.20}$$

where $L''(x) = \frac{\partial^2 L(x)}{\partial x^2}$ Consequently (2.15) will now be:

$$e^{L(x-1)} = e^{L(x)}e^{-L'(x)}e^{\frac{1}{2}L''(x)} \tag{2.21}$$

Eqn. (2.18) becomes

$$-\frac{\partial L(x)}{\partial x} + \frac{1}{2}\frac{\partial^2 L(x)}{\partial x^2} = \ln\frac{s+\alpha+\beta x}{\gamma+\beta x} \tag{2.22}$$

Differentiating (2.18), we have:

$$\frac{\partial^2 L(x)}{\partial x^2} = \beta\left[-\frac{1}{s+\alpha+\beta x} + \frac{1}{\gamma+\beta x}\right] \tag{2.23}$$

Hence Eqn. (2.22) becomes:

$$-\frac{\partial L(x)}{\partial x} = \ln\frac{s+\alpha+\beta x}{\gamma+\beta x} - \frac{\beta}{2}\left[-\frac{1}{s+\alpha+\beta x} + \frac{1}{\gamma+\beta x}\right] \tag{2.24}$$

Integrating (2.24) to give the second approximation:

$$\begin{aligned} L_2(x,s) = &-\int_x^{k'} \ln\frac{s+\alpha+\beta\omega}{\gamma+\beta\omega}\,\mathrm{d}\omega \\ &+ \ln\frac{[s+\alpha+\beta k']^{1/2}[\gamma+\beta x]^{1/2}}{[s+\alpha+\beta x]^{1/2}[\gamma+\beta k']^{1/2}[s+A^\dagger+Dk']} \end{aligned} \tag{2.25}$$

where

$$\int_{k'}^{x}\frac{\beta}{2}\left[-\frac{1}{s+\alpha+\beta\omega} + \frac{1}{\gamma+\beta\omega}\right]\mathrm{d}\omega = \ln\frac{[s+\alpha+\beta k']^{1/2}[\gamma+\beta x]^{1/2}}{[s+\alpha+\beta x]^{1/2}[\gamma+\beta k']^{1/2}}$$

To get the required expression for $P(x,t)$ one makes use of Eqn. (2.6b).

$$P_2(x,t) = \frac{1}{2\pi i}\int_{C-i\infty}^{C+i\infty} g(s)e^{st-f(s)}\,\mathrm{d}s \tag{2.26}$$

where

$$g(s) = \left[\frac{(s+\alpha+\beta k')(\gamma+\beta x)}{(s+\alpha+\beta x)(\gamma+\beta k')}\right]^{1/2} \frac{1}{(s+A^\dagger+Dk')} \tag{2.27a}$$

$$f(s) = \int_{k'}^{x} \ln \frac{s+\alpha+\beta\omega}{\gamma+\beta\omega}\,\mathrm{d}\omega \tag{2.27b}$$

Unfortunately, Eqn. (2.26) cannot be solved completely. An asymptotic solution is obtained using the saddle point approximation.

2.3.2 Saddle Point Approximation

The complete analysis of steepest descents involves choosing an integration path along a line of steepest descent from s_0, which can be obtained from the path in Eqn. (2.26). This particular treatment will lead to the following asymptotic form:

$$F(t) \sim \frac{g(s_0)e^{s_0 t - f(s_0)}}{[-2\pi f''(s_0)]^{1/2}} \tag{2.28}$$

which is used to approximate Eqns. (2.26) to (2.27b).

First, $f''(s_0)$ is obtained.

$$\begin{aligned} f''(s_0) &= \frac{\partial^2}{\partial s^2}\int_{k'}^{x} \ln\frac{s+\alpha+\beta\omega}{\gamma+\beta\omega}\,\mathrm{d}\omega\bigg|_{s=s_0} \\ &= \int_{k'}^{x} \frac{\partial^2}{\partial s^2}\ln\frac{s+\alpha+\beta\omega}{\gamma+\beta\omega}\bigg|_{s=s_0}\mathrm{d}\omega \\ &= -\int_{k'}^{x}\frac{1}{(s_0+\alpha+\beta\omega)^2}\,\mathrm{d}\omega \end{aligned} \tag{2.29}$$

Substituting this expression of $f''(s_0)$ and the values for $g(s_0)$ and $f(s_0)$ from (2.27a) and (2.27b) into (2.28), one arrives at:

$$P_2(x,t) = \frac{\left[\frac{(s_0+\alpha+\beta k')(\gamma+\beta x)}{(s_0+\alpha+\beta x)(\gamma+\beta k')}\right]^{1/2}\frac{1}{(s_0+A^\dagger+Dk')}}{\left[2\pi\int_{k'}^{x}\frac{1}{(s_0+\alpha+\beta\omega)^2}\,\mathrm{d}\omega\right]^{1/2}} \times e^{s_0 t - \int_{k'}^{x}\ln\frac{s_0+\alpha+\beta\omega}{\gamma+\beta\omega}\,\mathrm{d}\omega} \tag{2.30}$$

The equation can be broken down into three parts for simpler evaluation.

Let y represent the square root terms (except the 2π term) and z represent the exponential term, i.e., (2.30) can be written as:

$$P_2(x,t) = \frac{1}{(2\pi)^{1/2}} \frac{y\,z}{s_0 + A^\dagger + Dk'} \tag{2.31}$$

First, one considers the exponential term and look for a stationary function when the exponential term is stationary, i.e., $\frac{\partial z}{\partial s_0} = 0$. So,

$$\frac{\partial z}{\partial s_0} = \left(t - \int_{k'}^{x} \frac{1}{s_0 + \alpha + \beta\omega}\,\mathrm{d}\omega \right) \times z = 0 \tag{2.32}$$

Since $z \neq 0$ one immediately obtains:

$$\begin{aligned} t &= \int_{k'}^{x} \frac{1}{s_0 + \alpha + \beta\omega}\,\mathrm{d}\omega \\ &= \frac{1}{\beta} \ln\left[\frac{s_0 + \alpha + \beta x}{s_0 + \alpha + \beta k'} \right] \end{aligned} \tag{2.33}$$

Armed with this expression for t, one can simplify (2.30). Also note that:

$$e^{-\beta t} = \frac{s_0 + \alpha + \beta k'}{s_0 + \alpha + \beta x} \tag{2.34a}$$

and

$$1 - e^{-\beta t} = \frac{(x - k')\beta}{s_0 + \alpha + \beta x} \tag{2.34b}$$

Starting with the exponential term, let

$$\begin{aligned} u &= -\int_{k'}^{x} \ln \frac{s_0 + \alpha + \beta\omega}{\gamma + \beta\omega}\,\mathrm{d}\omega \\ &= \frac{1}{\beta} \left[\ln \left(\frac{(s_0 + \alpha + \beta k')^{s_0+\alpha+\beta k'}}{(s_0 + \alpha + \beta x)^{s_0+\alpha+\beta x}} \frac{(\gamma + \beta x)^{\gamma+\beta x}}{(\gamma + \beta k')^{\gamma+\beta k'}} \right) \right] \end{aligned}$$

Hence, $z = e^{s_0 t} e^{u}$.

$$z = \frac{e^{-t(\alpha+k'\beta)}(1 - e^{-\beta t})^{x-k'}}{(x - k')^{x-k'}} \frac{(k + x)^{k+x}}{(k + k')^{k+k'}} \tag{2.35}$$

where (2.34a) and (2.34b) have been used. Also, the substitution

$$k = \frac{\gamma}{\beta} \tag{2.36}$$

is made.

Next, the square root terms are evaluated. The integral in the denominator is:

$$\left[\int_{k'}^{x} \frac{1}{(s_0+\alpha+\beta\omega)^2}\,\mathrm{d}\omega\right]^{1/2} = \frac{(x-k')^{1/2}}{(s_0+\alpha+\beta k')^{1/2}(s_0+\alpha+\beta x)^{1/2}} \tag{2.37}$$

Combining this with the numerator, we have the expression for y.

$$y = (s_0+\alpha+\beta k')\left(\frac{(k+x)}{(x-k)(k+k')}\right)^{1/2} \tag{2.38}$$

we let $p = (s_0+\alpha+\beta k')$ and $q = \left(\frac{(k+x)}{(x-k)(k+k')}\right)^{1/2}$. Combining p with the $\frac{1}{s_0+A^\dagger+Dk'}$ term:

$$w = \frac{p}{s_0+A^\dagger+Dk'} = \frac{s_0+\alpha+\beta k'}{s_0+A^\dagger+Dk'} \tag{2.39}$$

Recalling $A^\dagger = \alpha + B$ and $D = \beta + B$,

$$w = \frac{e^{-\beta t}(x-k')}{\left[e^{-\beta t}(x-k') + \frac{B}{\beta}(1-e^{-\beta t})(1+k')\right]} \tag{2.40}$$

Thus, with (2.35) and (2.40) as well as an expression for q, Eqn. (2.31) will have the following form:

$$P_2(x_t) = \frac{e^{-t(\alpha+(k'+1)\beta)}(1-e^{-\beta t})^{x-k'}}{\left[e^{-\beta t}(x-k') + \frac{B}{\beta}(1-e^{-\beta t})(1+k')\right]} \times (x-k') \times \phi \tag{2.41}$$

where

$$\phi = \frac{(k+x)^{k+x+1/2}}{(2\pi)^{1/2}(x-k')^{x-k'+1/2}(k+k')^{k+k'+1/2}} \tag{2.42}$$

The ϕ term is now investigated. The term ϕ turns out to contain the Stirling

approximation of the form

$$P! = \frac{P^{P+1/2}}{e^P}(2\pi)^{1/2} \tag{2.43}$$

And hence,

$$\begin{aligned}\phi &= \frac{(x+k)!}{(x-k')!(k+k')!} \\ &= \frac{\Gamma(x+k+1)}{\Gamma(x-k'+1)\Gamma(k+k'+1)}\end{aligned} \tag{2.44}$$

where the identity $x! = \Gamma(x+1)$ has been used.[1]

So, the final form of the asymptotic solution of the branching equation (2.3) is obtained by substituting (2.44) into (2.41). The variable x is then replaced with n.

$$\boxed{\begin{aligned}P(n) =& \frac{e^{-t(\alpha+(k'+1)\beta)}(1-e^{-\beta t})^{n-k'}}{\left[e^{-\beta t}(n-k') + \frac{D-\beta}{\beta}(1-e^{-\beta t})(1+k')\right]} \times (n-k') \\ & \times \frac{\Gamma(n+k+1)}{\Gamma(n-k'+1)\Gamma(k+k'+1)}\end{aligned}} \tag{2.45}$$

This is the Asymptotic Solution to the QCD-parton Branching Equation. The solution is a probability distribution of the number of partons produced in a collision. The solution describes another multiplicity distribution.

Remark: There is an error in the original derivation of this solution found in [15] due to the error in the expression of Stirling's formula[2]. Thus the expression for $P(n)$ in the original paper differs slightly from what is shown above. Eqn. (2.45) is the corrected solution.

[1] Since k and k' are both interpreted in an average way, the gamma function used is defined as: $\Gamma(x) = \int_0^\infty t^{x-1}e^{-t}\,\mathrm{d}t$

[2] The correct expression for Stirling's formula was obtained from [16]

2.3.3 Relation to the Generalized Multiplicity Distribution

Now suppose the probability vertex $B = C = 0$, i.e. there is no quark pair creation and four-gluon vertices in the branching process, then Eqn. (2.45) will reduce to:

$$\boxed{P(n) = e^{-At(k'+\frac{\alpha}{\beta})} \left[1 - e^{-At}\right]^{n-k'} \frac{\Gamma(n+k+1)}{\Gamma(n-k'+1)\Gamma(k+k'+1)}} \tag{2.46}$$

The distribution described by Eqn. (2.46) is slightly different from the Generalized Multiplicity Distribution (GMD) due to the different expression for the parameter k. Under the condition $B = C = 0$, we have the relation that $\frac{\alpha}{\beta} = k_{\mathrm{GMD}}$ and $k_{\mathrm{GMD}} = k + 1$. Using these two relations reduce the distribution to the General Multiplicity Distribution.

$$P_{\mathrm{GMD}}(n) = e^{-At(k'+k_{\mathrm{GMD}})} \left[1 - e^{-At}\right]^{n-k'} \frac{\Gamma(n+k_{\mathrm{GMD}})}{\Gamma(n-k'+1)\Gamma(k_{\mathrm{GMD}}+k')} \tag{2.47}$$

2.4 Mean Multiplicity, Moments & KNO-Scaling

Since the asymptotic solution is a probability distribution, one makes use of certain statistics to characterize this distribution, in particular the mean and moments of the distribution. For example, the first moment is related to the mean, the second to the variance, the third to the skewness, the fourth to the kurtosis and so on. As noted, the mean multiplicity is the first moment of interest.

The mean multiplicity $\overline{n}$ is defined as:

$$\overline{n} = \sum_n n P_n \tag{2.48}$$

The reduced C-moment is defined as:

$$C_q = \frac{\overline{n^q}}{\overline{n}^q} = \frac{\sum_n n^q P_n}{(\sum_n n P_n)^q} \tag{2.49}$$

where $q \in \mathbb{Z}^+$.[3] Note that, per the definition from Eqn. (2.49), C_1 will always have the value of 1.

2.4.1 KNO-Scaling

The energy dependance of the multiplicity distributions and its moments have been discussed in relation to the so-called Koba-Nielsen-Olesen (KNO) scaling[17]. The main assumption of KNO scaling is that of Feynman scaling. According to Feynman scaling[18]:

$$\overline{n} \propto \ln \sqrt{s} \tag{2.50}$$

The derivation of KNO scaling is a result of an extension of Feynman scaling to include q-particle correlations (q-particles with energies E_q, momenta p_q).[4] The multiplicity distribution is found to scale as

$$P(n) = \frac{1}{\overline{n}} \Psi(\frac{n}{\overline{n}}) + \mathcal{O}\left(\frac{1}{\overline{n}^2}\right) \tag{2.51}$$

where the first term results in the leading term in $\ln s$, i.e. $(\ln s)^q$. All other terms in $\ln s$ ($(\ln s)^{q'}$ where $q' < q$) are contained in the second term.

This scheme involves the consideration of the function:

$$\Psi(z) = \overline{n} P_n \tag{2.52}$$

where $z = n/\overline{n}$. $\Psi(z)$ is a universal function, i.e. it is energy independent. If KNO scaling holds, multiplicity distributions of all energies fall on the same curve when plotted as a function of z[19,20]. Furthermore, it follows that the

[3] $\mathbb{Z}^+$ is the set of all positive integers, i.e. 1, 2, 3, 4...

[4] More on Feynman Scaling and KNO Scaling can be found in Appendix D

C_q moments define $\Psi(z)$ uniquely and are energy independent as well.

$$C_q = \int_0^\infty z^q \Psi(z)\,\mathrm{d}z \tag{2.53}$$

2.5 Summary

In this chapter, the Asymptotic Solution to the QCD-Parton Branching equation has been derived. The solution is obtained by considering four processes with their corresponding probabilities (in parenthesis):

i. gluon fission (A): $g \to g + g$,

ii. quark brehmsstrahlung ($\tilde{A}$): $q \to q + g$,

iii. quark pair creation (B): $g \to q + \bar{q}$,

iv. four gluon vertex (C): $g \to g + g + g$.

The parameters used are α, β, D, k, and k' which are defined as follows:

$$\alpha = A^\dagger - B$$

$$\beta = A + C$$

$$D = A + B + C$$

$$k = \frac{\gamma}{\beta} = \frac{A^\dagger - A - 2C}{A + C}$$

$$k' = \text{initial number of gluons}$$

The Asymptotic Solution is:

$$\begin{aligned} P(n) =& \frac{e^{-t(\alpha+(k'+1)\beta)}(1-e^{-\beta t})^{n-k'}}{\left[e^{-\beta t}(n-k') + \frac{D-\beta}{\beta}(1-e^{-\beta t})(1+k')\right]} \times (n-k') \\ & \times \frac{\Gamma(n+k+1)}{\Gamma(n-k'+1)\Gamma(k+k'+1)} \end{aligned} \tag{2.45}$$

The asymptotic solution reduces to the Generalized Multiplicity Distribution when $B = C = 0$.

Chapter 3

Data Analysis

In this work, proton-proton collision data from the Compact Muon Solenoid (CMS) experiment at the Large Hadron Collider (LHC), was analysed. In particular the charged particle multiplicity data at energies of 900 GeV, 2360 GeV and 7000 GeV were of interest. The data was obtained from The Durham HepData Project [20,21].

3.1 About the Data

Measurements of multiplicity distribution P_n of **primary charged hadrons** (baryons and mesons; although mostly π-mesons are produced in the collider) in **inelastic non-single-diffractive events** were performed at the Large Hadron Collider. These measurements were done at three center-of-mass energies, $\sqrt{s}$, of 900, 2360 and 7000 GeV, with pseudorapidity intervals of $|\eta| < 0.5$ to $|\eta| < 2.4$. For simplicity,the pseudorapidity cut η_c is defined as:

$$(\eta_c = x) \equiv |\eta| < x$$

i.e. $\eta_c = 0.5$ means $|\eta| < 0.5$. More information about η and $\sqrt{s}$ can be found in Appendix B.

3.1.1 Primary Interactions

Primary charged hadrons are defined as all charged hadrons produced in the interaction (collision), including products of the decay of objects with lifetime less than 10^{-10} s[20]. Decay products of longer-lived particles such as K^0_S and Λ, as well as hadrons originating from secondary interactions are excluded. Here, secondary interactions refer to any other interaction other than the initial proton-proton collision.

3.1.2 Non-Single-Diffractive (NSD) Events

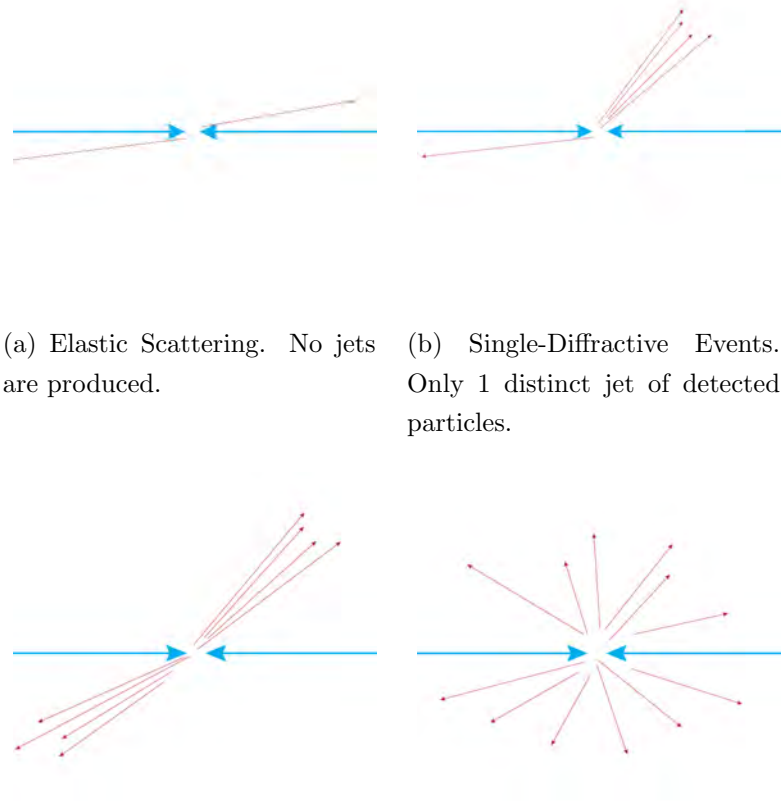

(a) Elastic Scattering. No jets are produced.

(b) Single-Diffractive Events. Only 1 distinct jet of detected particles.

(c) Double-Diffractive Events. Particles are produced in 2 jets.

(d) Non-Diffractive Events. Particles produced in all directions.

Figure 3.1: Different scattering events.

An explanation of non-single-diffractive (NSD) events is best done with Figure 3.1. The blue arrows indicate the colliding proton beams, whilst the red arrows indicate the "trajectories" of the particles.

Firstly, elastic events are events where no jets are produced. The proton's act like "billiard balls" and just glance off each other. Products of these type of collision have high η (close to the beam pipe) and will thus go undetected.

Inelastic events are categorised into diffractive events and non-diffractive events. Diffractive events have large rapidity intervals devoid of any hadronic activity. This interval is also known as the pseudorapidity gap. The two types of diffractive events, single-diffractive (SD) and double-diffractive (DD) are shown in Figures 3.1(b) and 3.1(c). All other inelastic events are known as non-diffractive (ND) events.

DD and ND events combined are known as non-single-diffractive (NSD) events. Event selection triggers are used to filter out events which do not fall into this category. The triggers also filter out events which are not due to primary interactions[20].

3.2 Analysis Methodology

In order to garner whether the data used can be described well by the distribution as expressed in Eqn. (2.45)[1], a χ^2-fit was used.

The χ^2 value is defined as such:

$$\chi^2 = \left(\frac{|P_{\text{ex}} - P_{\text{th}}|}{\sigma} \right)^2 \tag{3.1}$$

where P_{ex} is the experimental probabilities, P_{th} refers to the theoretical probabilities (as from Eqn. (2.45)), and σ is the experimental uncertainty.

It is often more useful to use the reduced χ^2 value,

$$\chi^2_{\text{red}} = \frac{\chi^2}{\nu} \tag{3.2}$$

[1]It may be puzzling to some as to why an equation that describes the behaviour of partons is used when the multiplicity distribution data refers to hadrons. The assumption of Local Parton-Hadron Duality has been used here (more of LPHD in Appendix C).

where $\nu = N_{\text{points}} - N_{\text{parameters}} - 1$ is the number of degrees of freedom. The reduced chi-squared value has an advantage in that it takes it normalizes for the number of points and takes into account model complexity.

This χ^2_{red} number was minimised to obtain the best fit of the data with the curve. The minimization and fit was done using the software OriginPro 9.0, which makes use of the Levenberg-Marquadt algorithm[2]. The fitting process was repeated for the pseudorapidity cuts of $\eta_c = 0.5$, 1.0, 1.5, 2.0, and 2.4 for each of the three energies of 900, 2360 and 7000 GeV. The points $n = 0$ and $n = 1$ were not included in the fit to allow k' ($n > k'$) to vary. The points at the tail end of the curve (high n) were also masked due to the high relative errors involved.

The fit parameters used are αt, βt, Dt, k and k'. The reason t was not used as a free parameter is because it does not appear independently of the α, β and D. Thus, the curve is over-parameterised if t is taken to be a free parameter, i.e. more parameters than are necessary to define the curve are used. However, the value of t can be considered as absorbed into that of α, β and D without any loss of generality. As such, for the sake of simplicity, the parameters αt, βt, and Dt can simply be written as α, β and D.

Also, since Eqns. (2.48) and (2.49) are difficult to evaluate analytically, they are done numerically. Once the fit parameters were obtained from the fit, $\overline{n}$ and the C_q moments were computed. The C_q moments were computed for $q = 2$, 3, 4, 5. Renormalization was performed before $\overline{n}$ and the C_q moments were calculated.

[2]A detailed description of the Levenberg-Marquadt algorithim can be found in [22]

3.3 Analysis of Multiplicity Data for $\sqrt{s} = 900$ GeV

The graphs in Figure 3.2 show the multiplicity distribution at 900 GeV for different η_c. Also shown on the graphs are the fit lines which were obtained with the asymptotic solution (Eqn. 2.45). The grey points are masked.

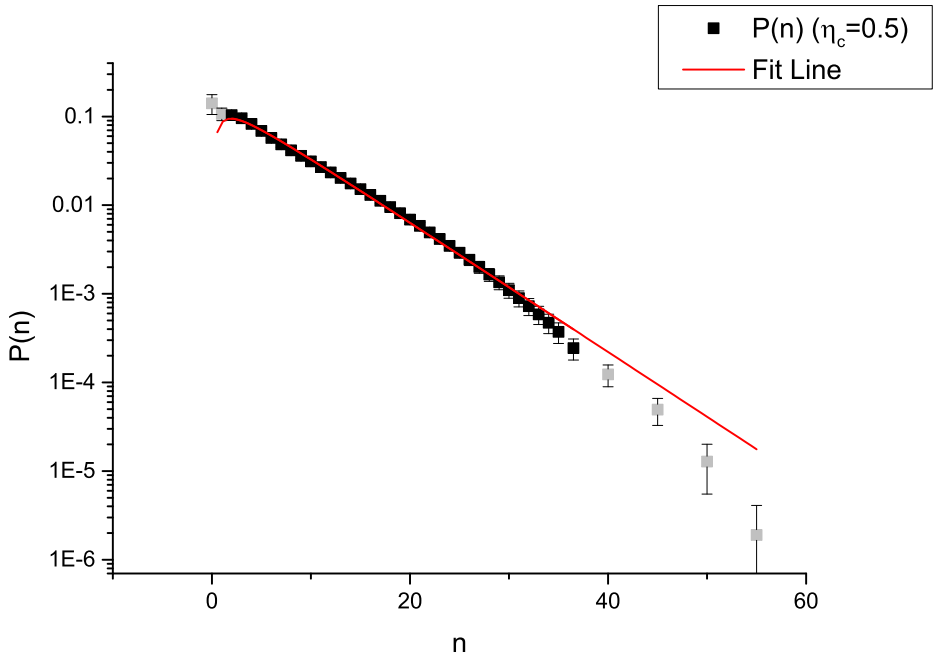

(a) Multiplicity distribution and asymptotic solution fit at $\eta_c = 0.5$.

Figure 3.2: Multiplicity distribution at 900 GeV for various η_c fitted with the Asymptotic Solution.

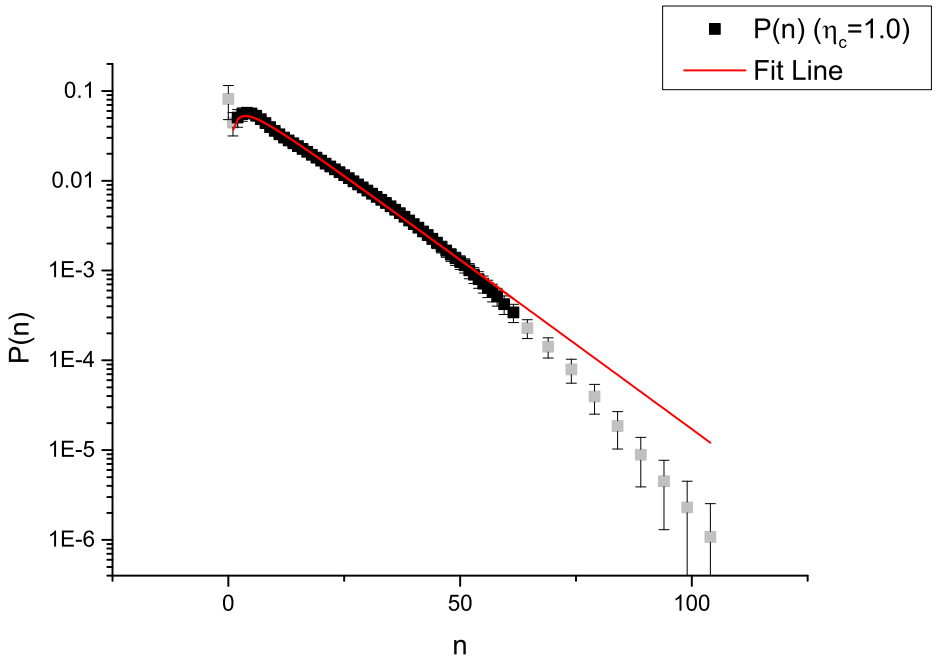

(b) Multiplicity distribution and asymptotic solution fit at $\eta_c = 1.0$.

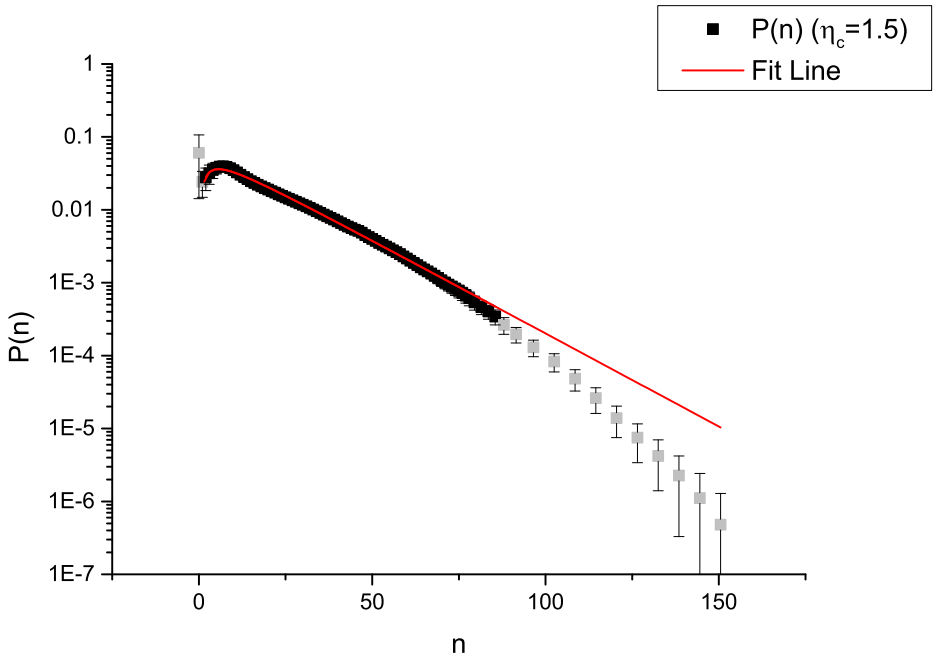

(c) Multiplicity distribution and asymptotic solution fit at $\eta_c = 1.5$.

Figure 3.2: Multiplicity distribution at 900 GeV for various η_c fitted with the Asymptotic Solution.

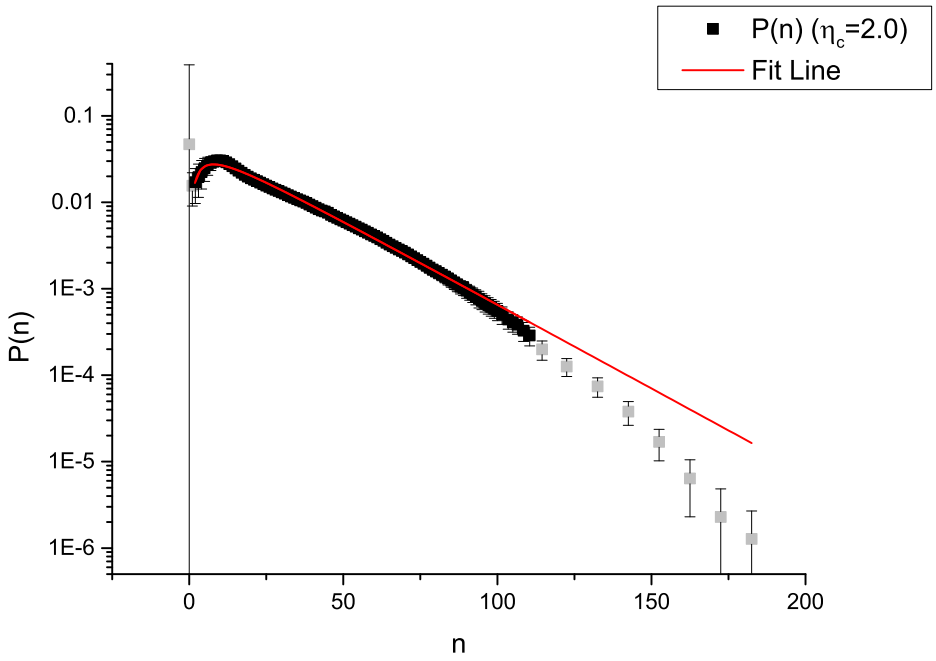

(d) Multiplicity distribution and asymptotic solution fit at $\eta_c = 2.0$.

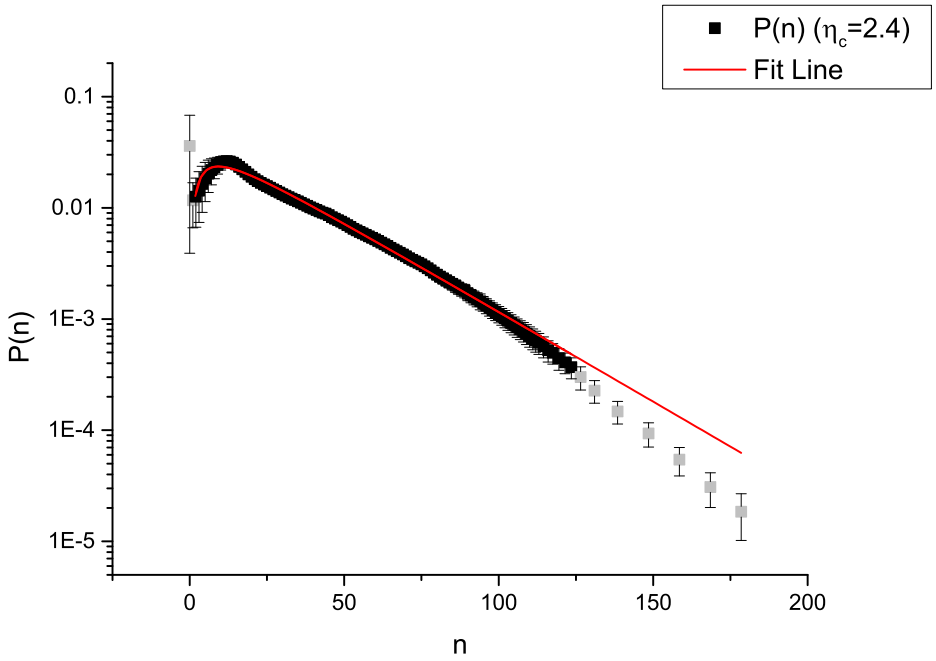

(e) Multiplicity distribution and asymptotic solution fit at $\eta_c = 2.4$.

Figure 3.2: Multiplicity distribution at 900 GeV for various η_c fitted with the Asymptotic Solution.

Table 3.1 summarises the fit parameters and the χ^2_{red} values for the fits across all η_c. The values of all these parameters increase as η_c increases. Also, $\chi^2_{\text{red}} < 1$ for all fits. The values of k' are very small compared compared

η_c	α	β	D	k	k'	χ^2_{red}
0.5	0.73	1.32	2.13	0.16	3.74×10^{-15}	0.91
1.0	0.99	1.82	3.64	0.54	4.00×10^{-15}	0.59
1.5	1.31	2.17	4.34	0.60	5.00×10^{-15}	0.50
2.0	1.53	2.42	4.85	0.63	7.00×10^{-15}	0.46
2.4	1.68	2.59	5.18	0.65	9.00×10^{-15}	0.39

Table 3.1: Fit Parameters for $\sqrt{s} = 900$ GeV at various η_c.

to that of k. Although there is an increasing trend across pseudorapidity, the value of k' is very small; they can be approximated as being constantly zero. Recall that k' is the initial number of gluons produced after collision. The parameter k is related to the number of quarks.[3] Thus both the initial number of gluons and quarks increases as η_c increases.

The values of α, β and D show an increasing trend with increasing η_c. From the definitions of α, β and D (Eqns. (2.17a), (2.17b), and (2.17d)), one notes that:

- Quark brehmmstrahlung ($A^\dagger$) dominates over quark pair creation (B) with increasing η_c (increasing α)
- Gluon splitting (gluon fission (A) and 4-gluon vertex (C)) increases as η_c increases (increasing β)
- Gluon initiated processes (gluon splitting and quark pair creation) increases as η_c increases (D increases)
- From the first three points, we can conclude that although all processes increase with η_c the quark brehmmstrahlung process (producing gluon

[3]If one uses the GMD as an example, k_{GMD} is defined as $k_{\text{GMD}} = \frac{A^\dagger}{A} = \frac{m\tilde{A}}{A}$. k is thus the number of quarks m multiplied by the ratio of the processes $\tilde{A}$ and A. Since k reduces to k_{GMD} when $B = C = 0$ (up to an additive constant), one can interpret k as being related to the number of quarks.

from quarks) increases much faster than the quark pair creation process (producing quarks from gluons).

The results indicate that as more particles are being considered (larger angle coverage), the processes producing gluons seem to become more likely as compared to those which produce quarks. Also, since the pseudorapidity (and hence angle) is related to the particles transverse momentum, a larger η_c means that particles with a larger range of transverse momenta are considered.

The mean multiplicity and the C_q moments that were numerically calculated from the fit parameters are shown in Table 3.2. Comparison between the experimental C_q moments and the calculated values are shown graphically in Figure 3.3.

As expected, $\overline{n}$ increases with increasing η_c. Referring to Figure 3.3, one can see that the C_q moments for $q = 2$, 3, 4 agree reasonably well with the experimental values. The values for C_5 however did not agree as well with the data. The difference in C_5 can be attributed to the difference at the tail section (high n values) of the distribution. Also, there seems to be less agreement of the C_q moments at higher η_c.

η_c	$\overline{n}$	C_2	C_3	C_4	C_5
0.5	4.46	1.57	3.36	8.91	27.52
1.0	8.19	1.55	3.22	8.20	24.23
1.5	11.84	1.54	3.14	7.74	21.94
2.0	15.38	1.53	3.04	7.24	19.59
2.4	18.09	1.51	2.94	6.79	17.71

Table 3.2: Mean Multiplicity and C_q moments for $\sqrt{s} = 900$ GeV.

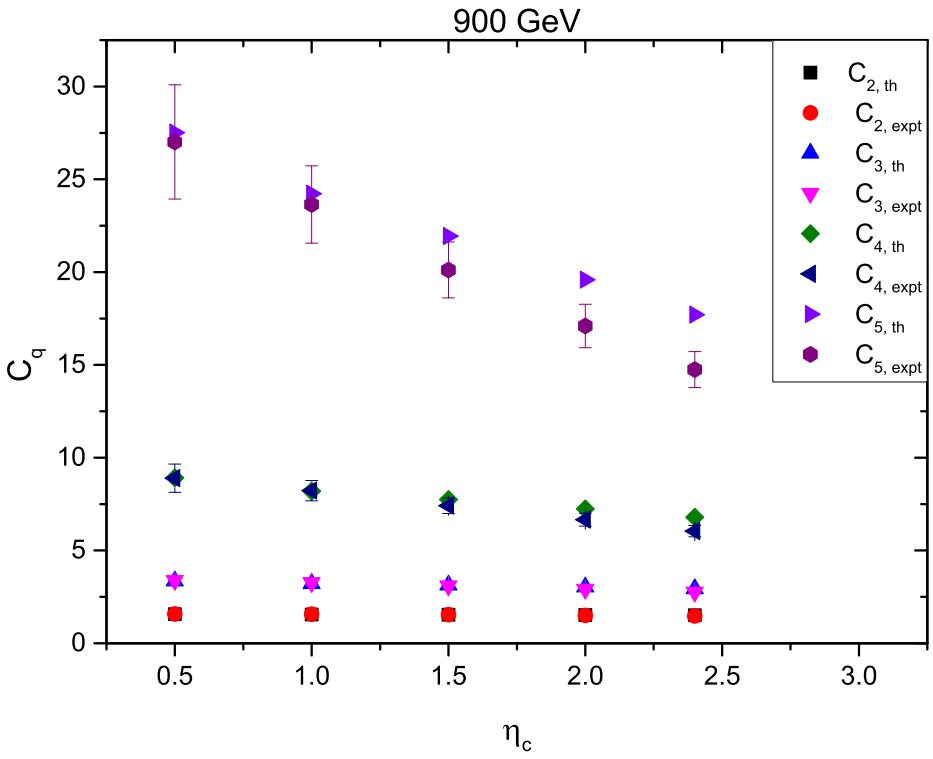

Figure 3.3: Comparison of experimental and theoretical C_q moments for 900 GeV.

3.4 Analysis of Multiplicity Data for $\sqrt{s} = 2360$ GeV

The graphs in Figure 3.4 exhibit the multiplicity distribution at 2360 GeV for different η_c. Also shown on the graphs are the fit lines which were obtained with the asymptotic solution (Eqn. 2.45). As before, the grey points are masked.

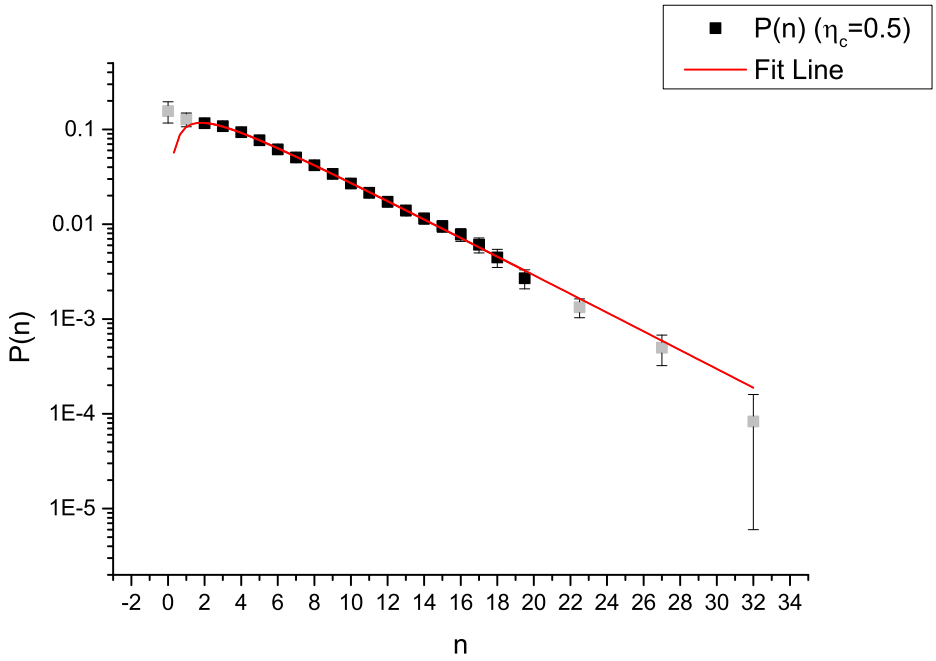

(a) Multiplicity distribution and asymptotic solution fit at $\eta_c = 0.5$.

Figure 3.4: Multiplicity distribution at 2360 GeV for various η_c fitted with the Asymptotic Solution.

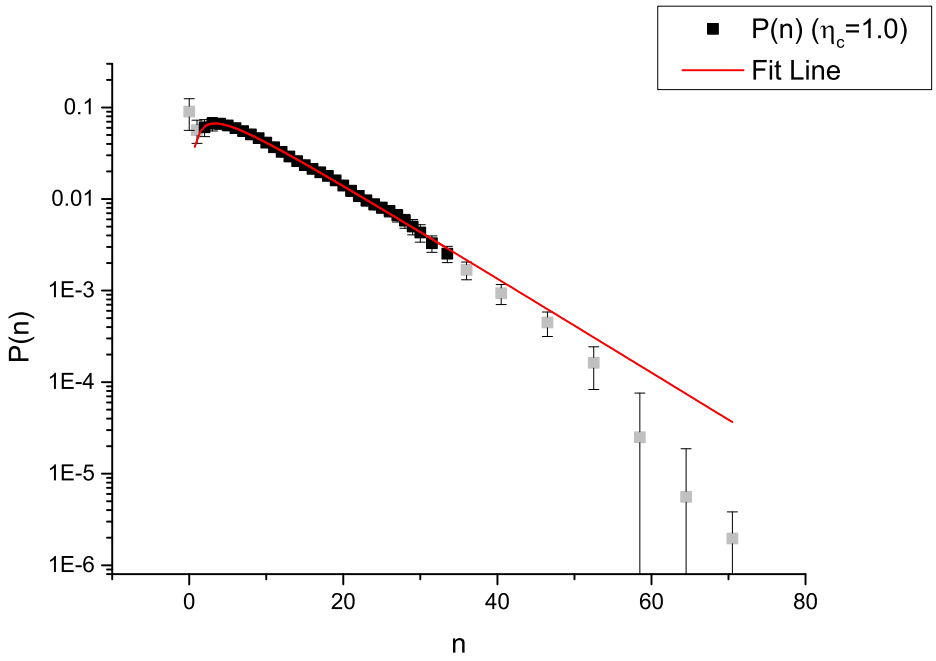

(b) Multiplicity distribution and asymptotic solution fit at $\eta_c = 1.0$.

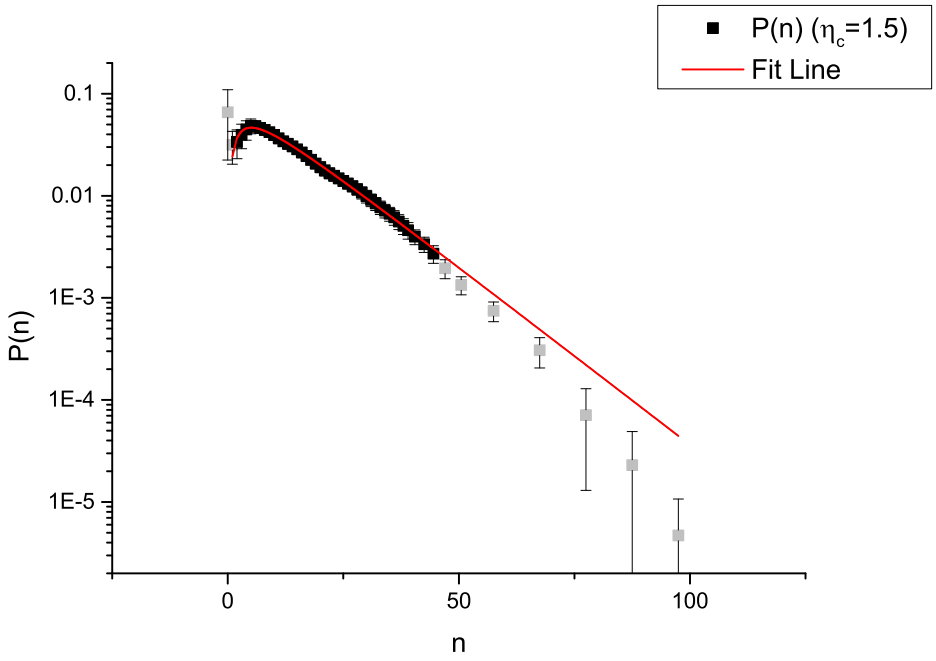

(c) Multiplicity distribution and asymptotic solution fit at $\eta_c = 1.5$.

Figure 3.4: Multiplicity distribution at 2360 GeV for various η_c fitted with the Asymptotic Solution.

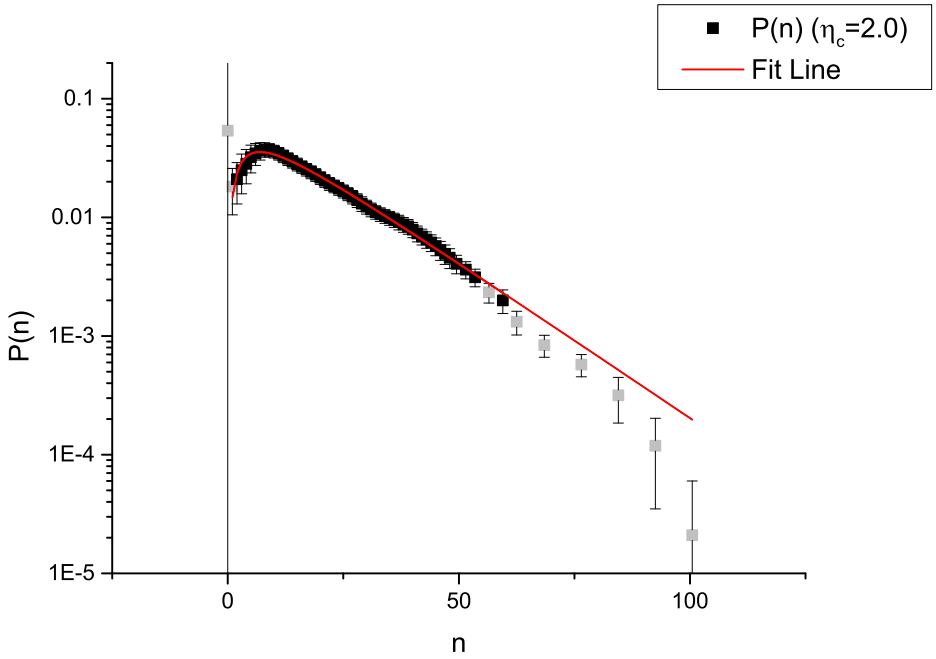

(d) Multiplicity distribution and asymptotic solution fit at $\eta_c = 2.0$.

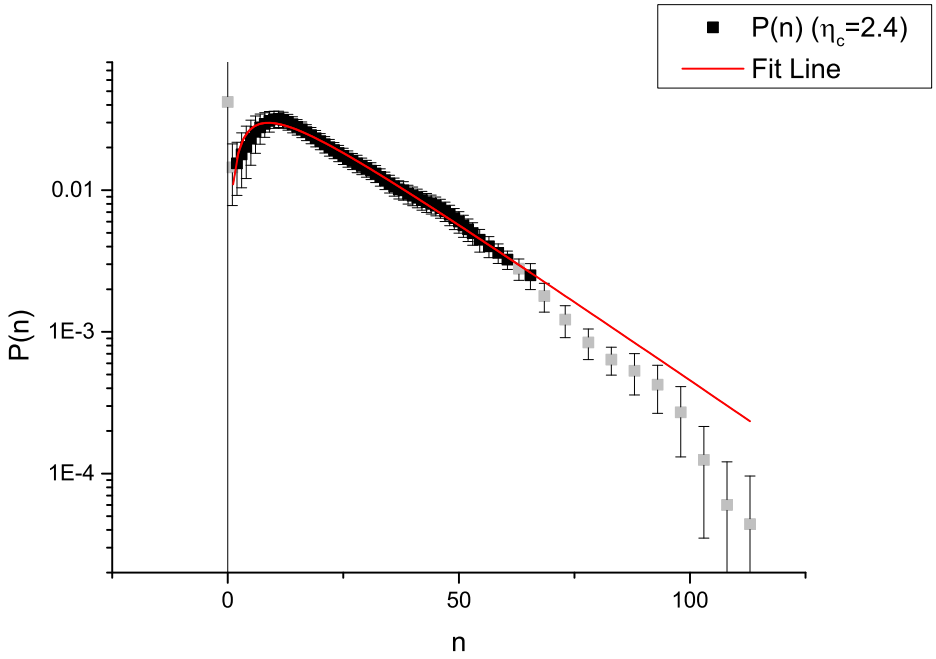

(e) Multiplicity distribution and asymptotic solution fit at $\eta_c = 2.4$.

Figure 3.4: Multiplicity distribution at 2360 GeV for various η_c fitted with the Asymptotic Solution.

Table 3.3 summarises the fit parameters and the χ^2_{red} values for the fits across all η_c. The values of all these parameters increase as η_c increases, as was the case with the data for 900 GeV. Also, $\chi^2_{\text{red}} < 0.2$ for all fits - indicating a good fit.

η_c	α	β	D	k	k'	χ^2_{red}
0.5	1.19	1.58	2.11	0.08	8.29×10^{-14}	0.13
1.0	1.80	2.19	2.80	0.10	4.30×10^{-14}	0.08
1.5	2.14	2.56	3.30	0.13	1.03×10^{-13}	0.08
2.0	2.37	2.83	3.73	0.15	1.14×10^{-13}	0.11
2.4	2.45	2.99	4.14	0.21	2.58×10^{-13}	0.11

Table 3.3: Fit Parameters for $\sqrt{s} = 2360$ GeV at various η_c.

The same analysis performed on the 900 GeV data set can be applied to this particular data set. As before, there is a trend that the values of the parameters increase as η_c increases. This is true for all the parameters execpt k'. The value of k' at $\eta_c = 0.5$ is slightly larger than that of $k' = 1.0$. However, as previously mentioned, the values of k' are orders of magnitude smaller than that of the other parameters. Thus this small difference could be treated as an anomalous result.

Since the values of α, β, D and k increase as η_c increases, the results from the previous analysis hold true as well.

Table 3.4 displays the mean multiplicity as well as the calculated C_q moments, while Figure 3.5 compares these calculated values with experimental values. From Figure 3.5, one can see that the values C_2, C_3, C_4 agree reasonably well, but again the values of C_5 differ from that of experimental values. In fact, these calculated values of C_5 display an odd behaviour as η_c increases. From the plot, one notices that C_5 should decrease with increasing η_c, but the calculated value of C_5 does not exhibit this behaviour. The possible anomalous points are at $\eta_c = 0.5$ and $\eta_c = 2.4$.

η_c	$\overline{n}$	C_2	C_3	C_4	C_5
0.5	5.41	1.56	3.25	8.22	24.15
1.0	9.87	1.56	3.23	8.17	24.56
1.5	14.11	1.53	3.03	7.26	20.54
2.0	18.39	1.51	2.92	6.78	18.36
2.4	21.83	1.50	2.90	6.83	18.97

Table 3.4: Mean Multiplicity and C_q moments for $\sqrt{s} = 2360$ GeV.

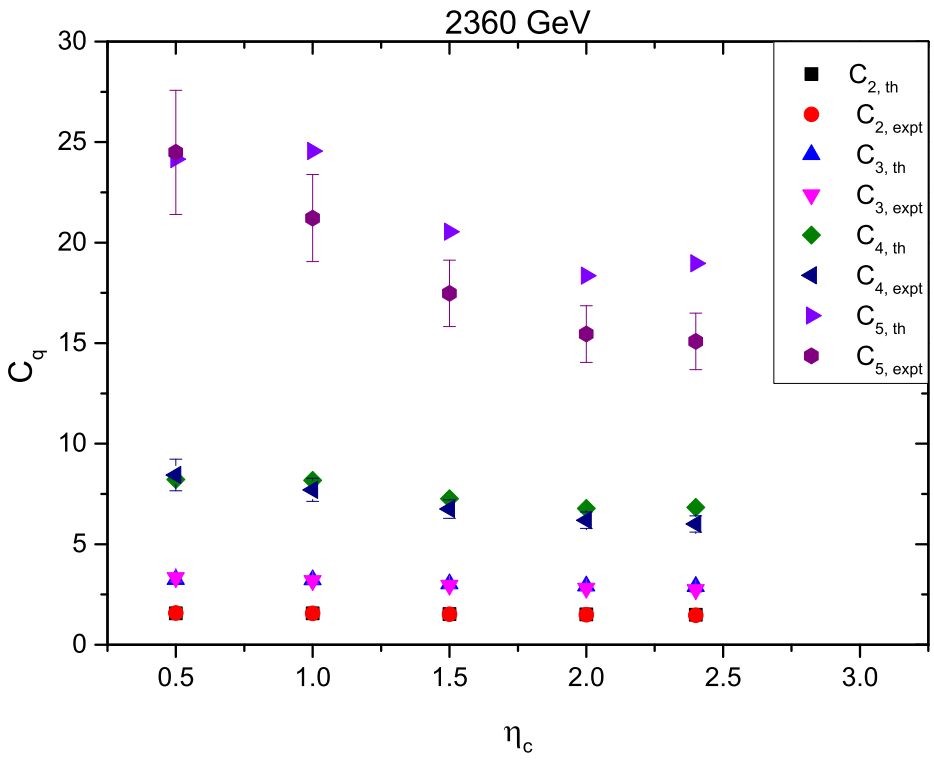

Figure 3.5: Comparison of experimental and theoretical C_q moments for 2360 GeV.

3.5 Analysis of Multiplicity Data for $\sqrt{s} = 7000$ GeV

The graphs in Figure 3.6 display the multiplicity distribution at 900 GeV for different η_c. Also shown on the graphs are the fit lines which were obtained with the asymptotic solution (Eqn. 2.45).

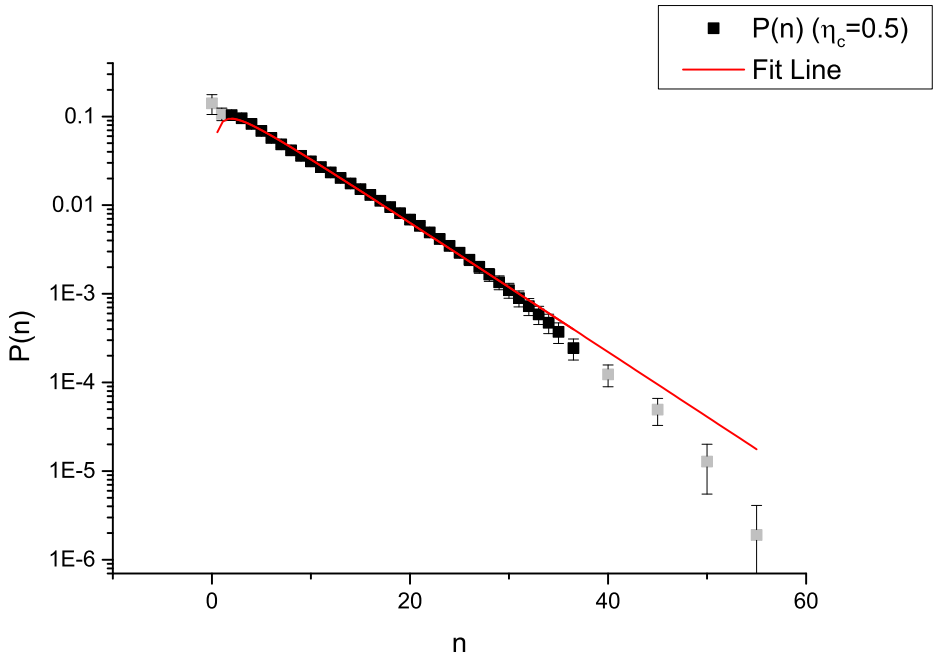

(a) Multiplicity distribution and asymptotic solution fit at $\eta_c = 0.5$.

Figure 3.6: Multiplicity distribution at 7000 GeV for various η_c fitted with the Asymptotic Solution.

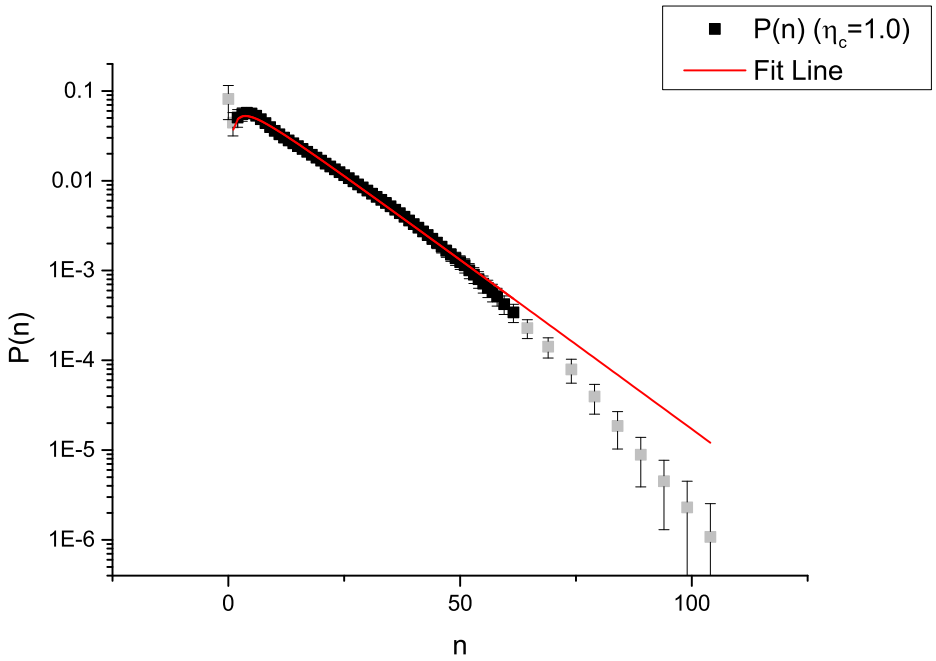

(b) Multiplicity distribution and asymptotic solution fit at $\eta_c = 1.0$.

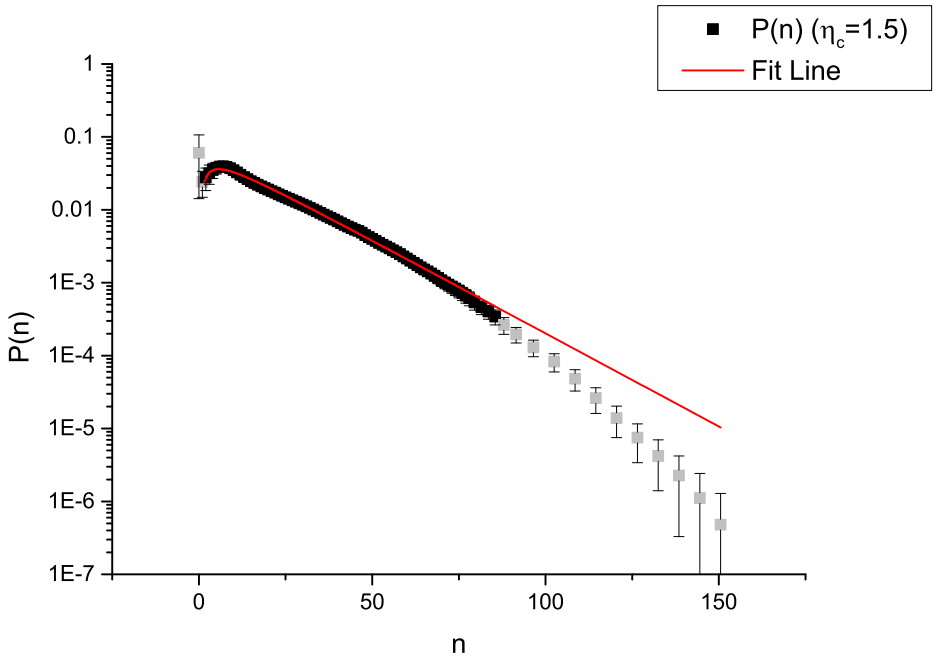

(c) Multiplicity distribution and asymptotic solution fit at $\eta_c = 1.5$.

Figure 3.6: Multiplicity distribution at 7000 GeV for various η_c fitted with the Asymptotic Solution.

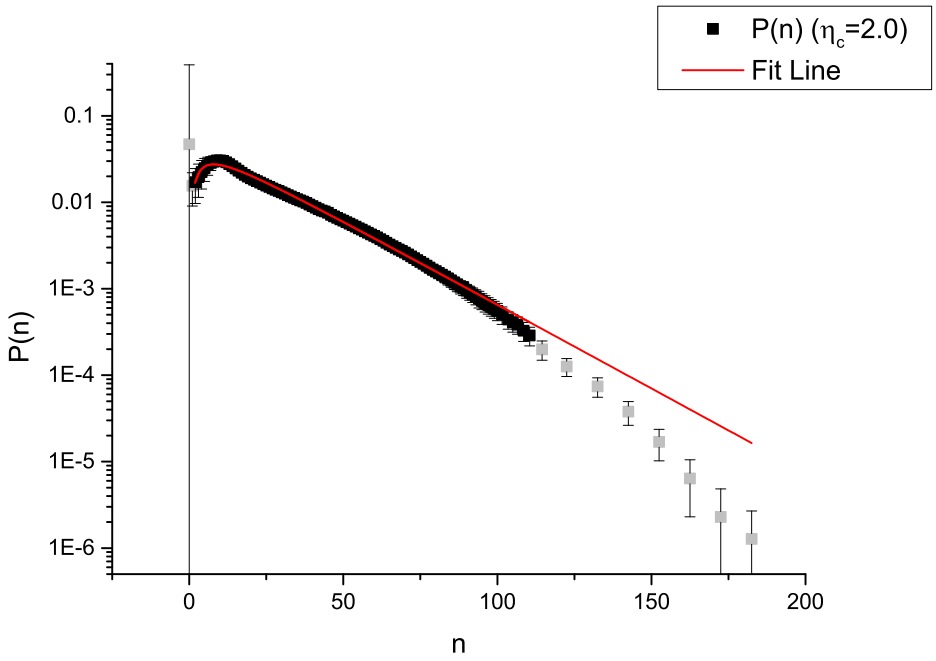

(d) Multiplicity distribution and asymptotic solution fit at $\eta_c = 2.0$.

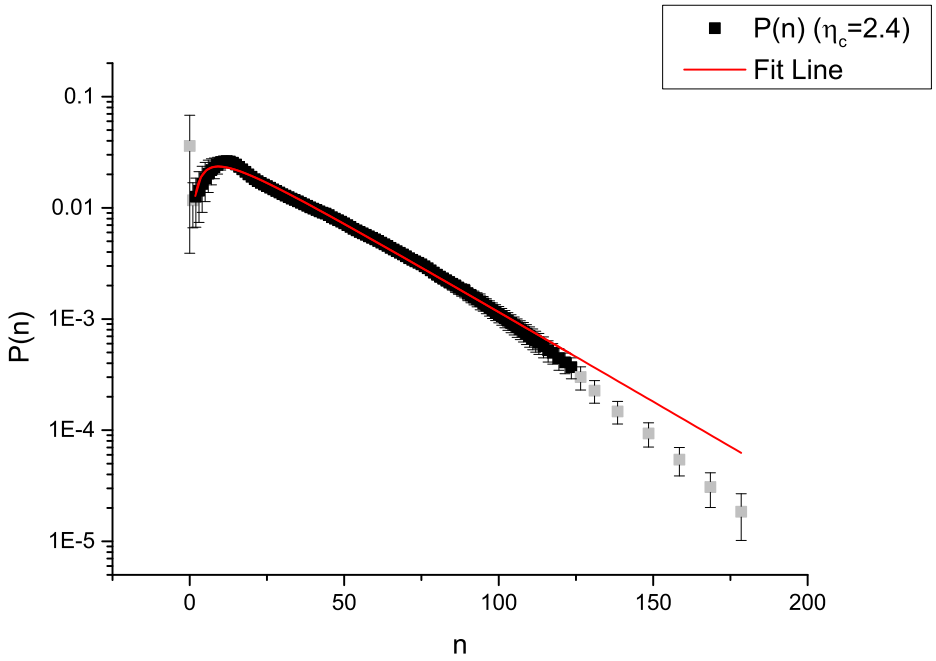

(e) Multiplicity distribution and asymptotic solution fit at $\eta_c = 2.4$.

Figure 3.6: Multiplicity distribution at 7000 GeV for various η_c fitted with the Asymptotic Solution.

Table 3.5 summarises the fit parameters and the χ^2_{red} values for the fits across all η_c. The parameters α, β, D and k' increase as η_c increases, whilst k decreases with increasing η_c. $\chi^2_{\text{red}} < 1$ for all η_c. The only difference in

η_c	α	β	D	k	k'	χ^2_{red}
0.5	1.64	1.86	2.18	9.63×10^{-03}	4.54×10^{-10}	0.91
1.0	2.24	2.48	2.87	7.62×10^{-03}	3.04×10^{-09}	0.59
1.5	2.58	2.86	3.35	6.49×10^{-03}	8.00×10^{-09}	0.50
2.0	2.81	3.13	3.74	2.15×10^{-03}	5.98×10^{-08}	0.46
2.4	2.97	3.30	3.93	1.09×10^{-04}	1.43×10^{-04}	0.39

Table 3.5: Fit Parameters for $\sqrt{s} = 7000$ GeV at various η_c.

the trend of parameters with increasing η_c of this data set and the former two is that of the parameter k. The value of k decreases with increasing η_c. An interesting point to note is also the value of k' at $\eta_c = 2.4$. There is a significant "jump" between that value and the preceding value. If one interprets k as being related to the number of quarks, it is clear that at this energy, the number of quarks decreases with increasing number of gluons. This is an indication that gluon processes start to dominate.

The calculated mean and moments are shown in Table 3.6 with the corresponding comparison plot on Figure 3.7. Again, one notes that the agreement of C_2, C_3, and C_4 is quite good; C_5 deviates slightly from the experimental values.

η_c	$\overline{n}$	C_2	C_3	C_4	C_5
0.5	7.13	1.69	3.98	11.72	40.51
1.0	13.42	1.68	3.91	11.19	37.44
1.5	19.76	1.66	3.75	10.36	33.31
2.0	26.16	1.64	3.59	9.51	28.85
2.4	30.91	1.62	3.50	9.01	26.27

Table 3.6: Mean Multiplicity and C_q moments for $\sqrt{s} = 7000$ GeV.

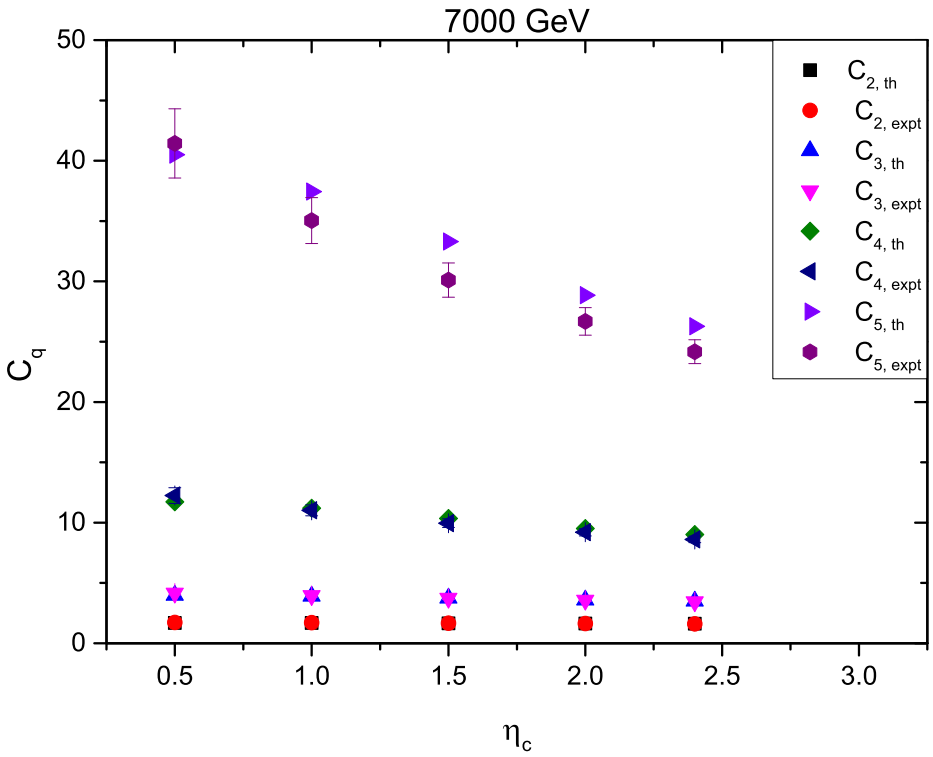

Figure 3.7: Comparison of experimental and theoretical C_q moments for 7000 GeV.

3.6 Comparison Across Energies

A comparison of the fit parameters across the three different centre-of-momentum frame energies was made. Tables 3.7 to 3.11 contain the values of the parameters across different energies and η_c. Each table corresponds to one parameter. Figure 3.8 displays these values graphically.

	$\boldsymbol{\alpha}$				
$\sqrt{s}$ (GeV)	η_c				
	0.5	1.0	1.5	2.0	2.4
900	0.73	0.99	1.31	1.53	1.68
2360	1.19	1.80	2.14	2.37	2.45
7000	1.64	2.24	2.58	2.81	2.97

Table 3.7: Comparison of α across different energies.

	$\boldsymbol{\beta}$				
$\sqrt{s}$ (GeV)	η_c				
	0.5	1.0	1.5	2.0	2.4
900	1.32	1.82	2.17	2.42	2.59
2360	1.58	2.19	2.56	2.83	2.99
7000	1.86	2.48	2.86	3.13	3.30

Table 3.8: Comparison of β across different energies.

	$\boldsymbol{D}$				
$\sqrt{s}$ (GeV)	η_c				
	0.5	1.0	1.5	2.0	2.4
900	2.13	3.64	4.34	4.85	5.18
2360	2.11	2.80	3.30	3.73	4.14
7000	2.18	2.87	3.35	3.74	3.93

Table 3.9: Comparison of D across different energies.

$\sqrt{s}$ (GeV)	k				
	η_c				
	0.5	1.0	1.5	2.0	2.4
900	0.16	0.54	0.60	0.63	0.65
2360	0.08	0.10	0.13	0.15	0.21
7000	9.63×10^{-03}	7.62×10^{-03}	6.49×10^{-03}	2.15×10^{-03}	1.09×10^{-04}

Table 3.10: Comparison of k across different energies.

$\sqrt{s}$ (GeV)	k'				
	η_c				
	0.5	1.0	1.5	2.0	2.4
900	3.74×10^{-15}	4.00×10^{-15}	5.00×10^{-15}	7.00×10^{-15}	9.00×10^{-15}
2360	8.29×10^{-14}	4.30×10^{-14}	1.03×10^{-13}	1.14×10^{-13}	2.58×10^{-13}
7000	4.54×10^{-10}	3.04×10^{-09}	8.00×10^{-09}	5.98×10^{-08}	1.43×10^{-04}

Table 3.11: Comparison of k' across different energies.

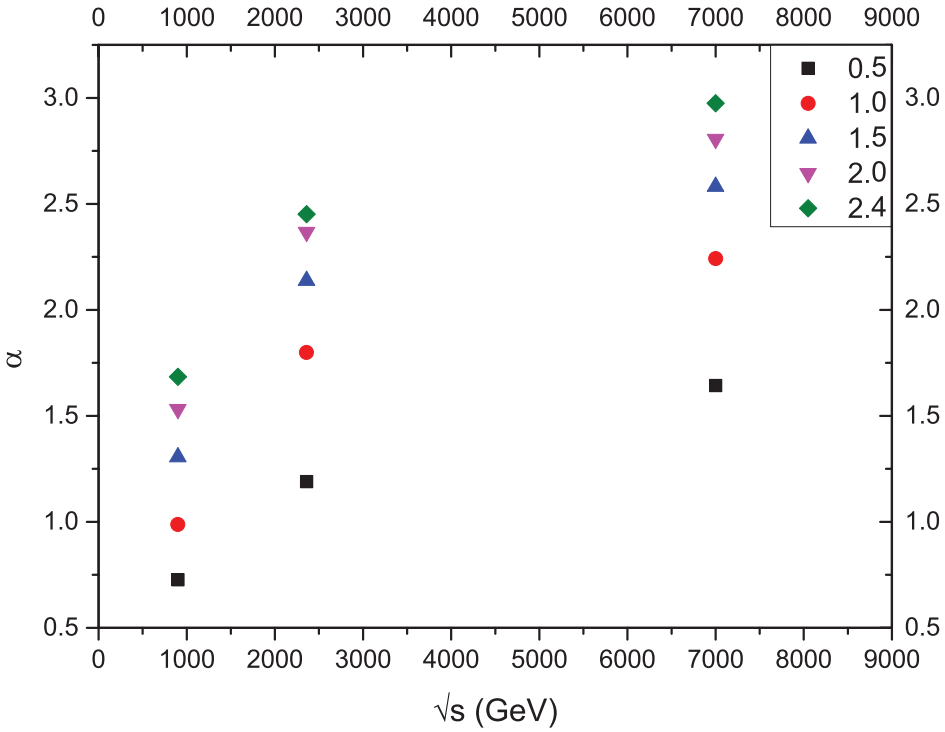

(a) Comparison of α across energies

Figure 3.8: Comparison of Fit Parameters Across Different Energies

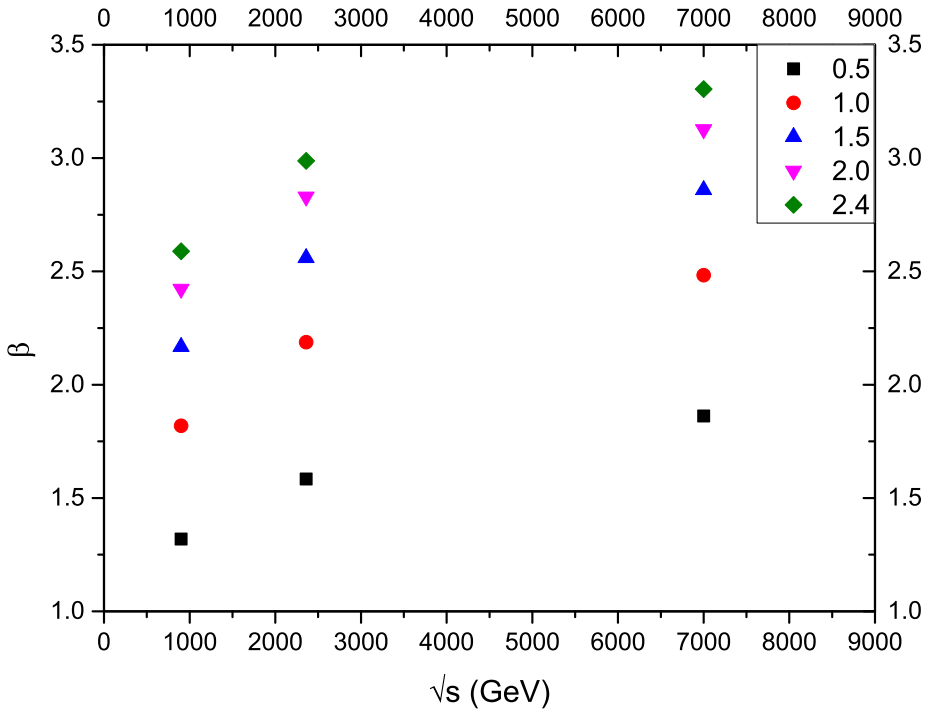

(b) Comparison of β across energies

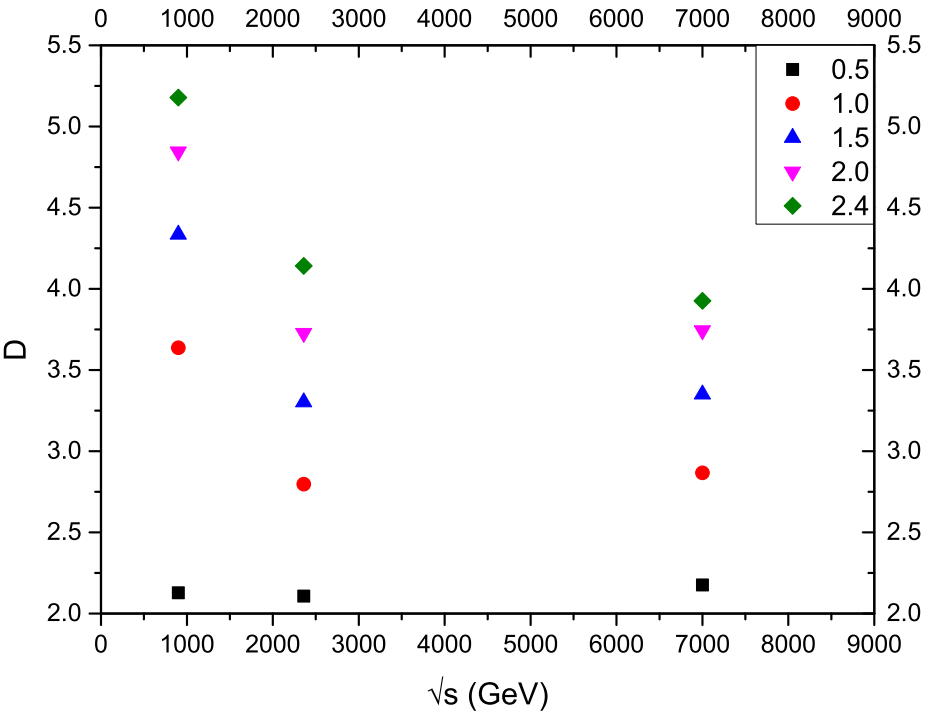

(c) Comparison of D across energies

Figure 3.8: Comparison of Fit Parameters Across Different Energies

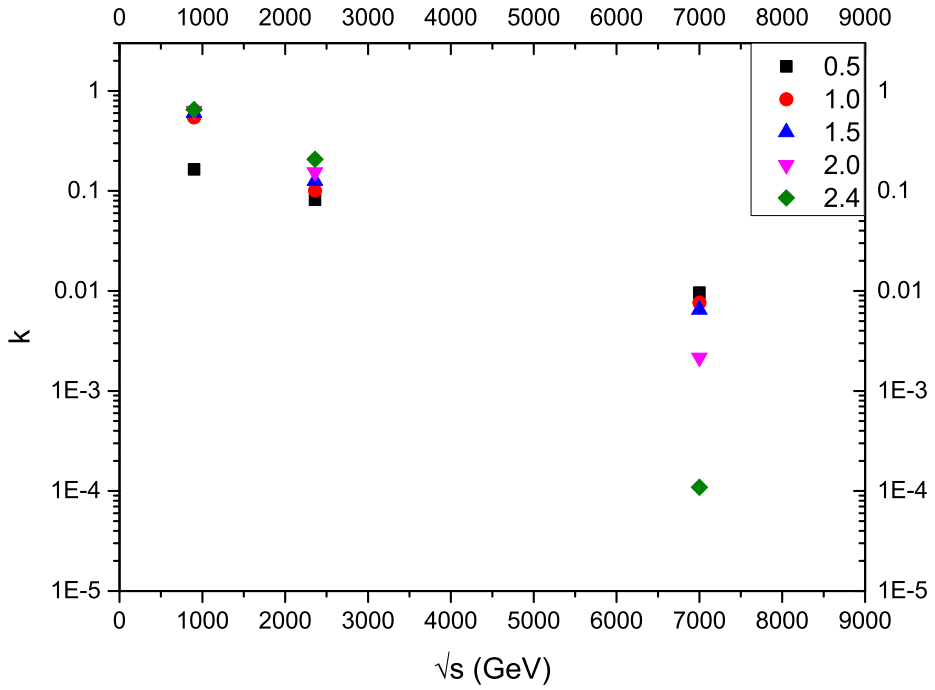

(d) Comparison of k across energies

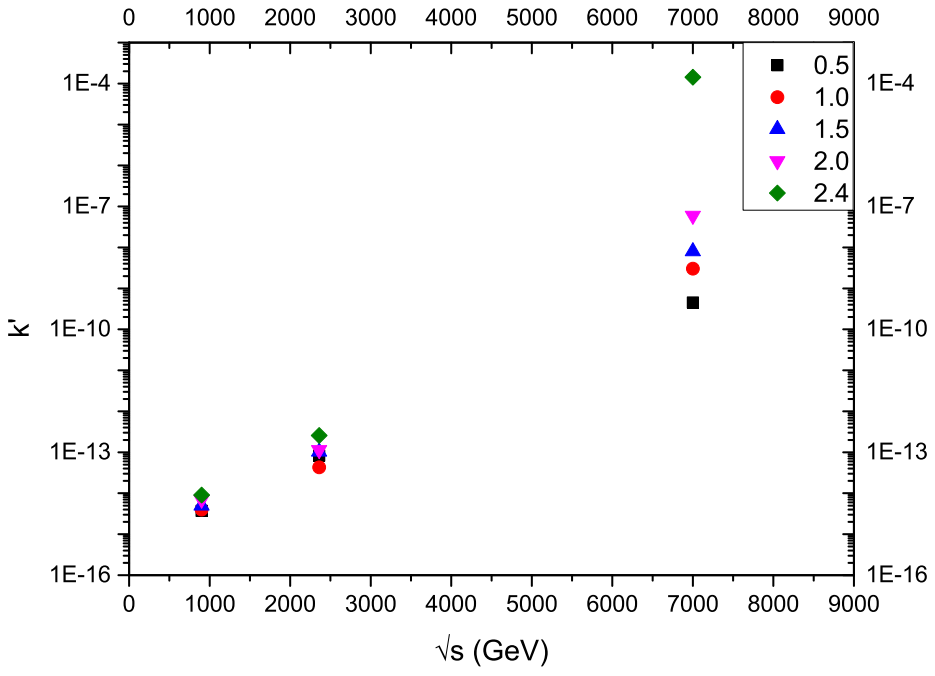

(e) Comparison of k' across energies

Figure 3.8: Comparison of Fit Parameters Across Different Energies

The behaviour of α and β across the energies is very similar. At each η_c the value for these two parameters increases. Thus, one infers that:

- Gluon brehmmstrahlung process ($A^\dagger$) increases more than that of quark pair-creation when energy increases.
- Gluon splitting (A and C) increases with the increase of energy.

Next, one looks at the behaviour of k and k'. As energy increases, k decreases, whilst k' increases. This leads to:

- The number of quarks decreases while the initial number of gluons increases.
- At higher energies, the gluon processes play a more dominant role over the quark processes.

Finally, one turns to the behaviour of D across the three energies. The parameter D behaves strangely. For η_c values of 0.5 to 2.0, as energy is increased from 900 GeV to 2360 GeV, the values of D decreases. Then as the energy is further increased to 7000 GeV, the values of D increase. This indicates a presence of some sort of minimum value of D between energy values of 2360 and 7000 GeV. On the other hand, values of D for $\eta_c = 2.4$ decreases with increasing energy. However, the behaviour of D for $\eta_c = 2.4$ is still consistent with the presence of a minima. The exact behaviour of D can only be determined with additional data at higher energies.

A possible inference for a minima behaviour of D is as follows. The variable D can be expressed as $D = \beta + B$. From the data, we know that β increases with increasing energy. For a decreasing portion of D, since β increases, B must decrease, and at a faster rate as compared to β. The increasing portion of the curve would indicate that if B decreases, then β would have to increase at a higher rate than the decreasing B.

Physically, this means that there seems to be a competition between the gluon splitting process ($\beta = A + C$) and the quark pair creation process (B). Initially, the quark pair creation process dominates. But at a certain energy (the minima point), the gluon processes start to dominate. This again is

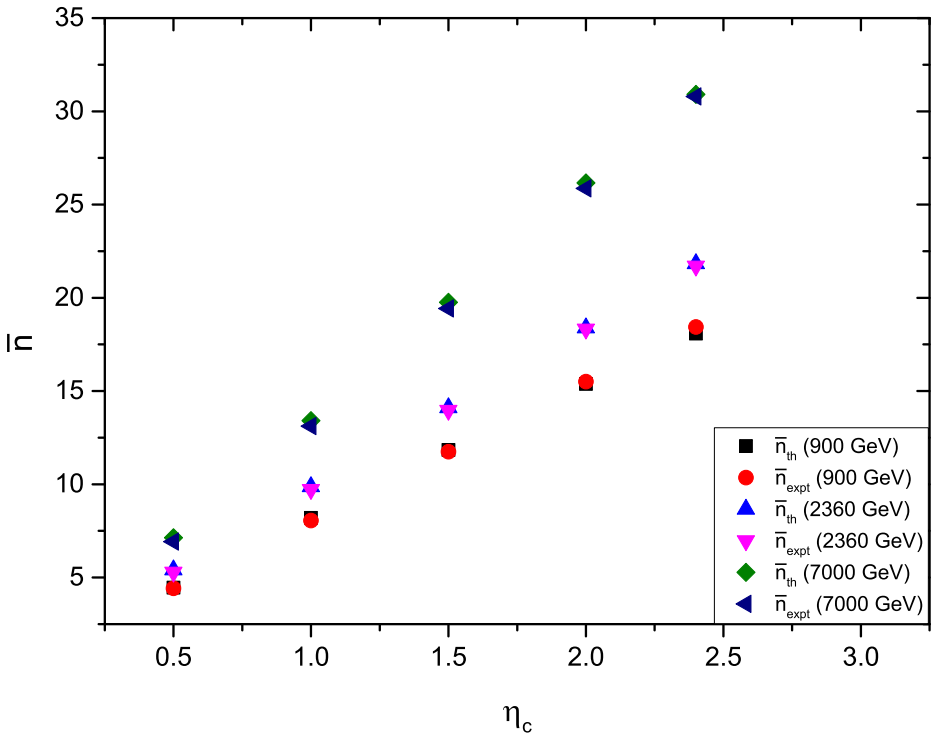

Figure 3.9: Comparison of $\overline{n}$ across different energies and η_c.

consistent with the assumption that at high energies, gluon processes will play a more significant role.

Turning ones attention to the mean multiplicity, the values of $\overline{n}$ across different energies are compared in Figure 3.9. The mean multiplicity increases as energy increases for each η_c.

3.6.1 Violation of KNO Scaling

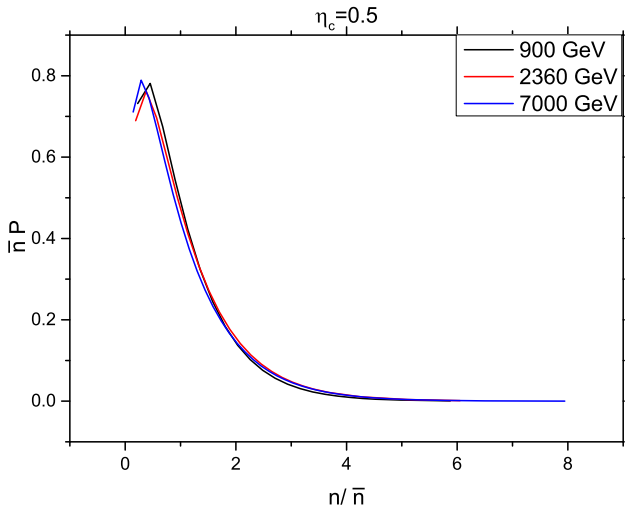

(a)

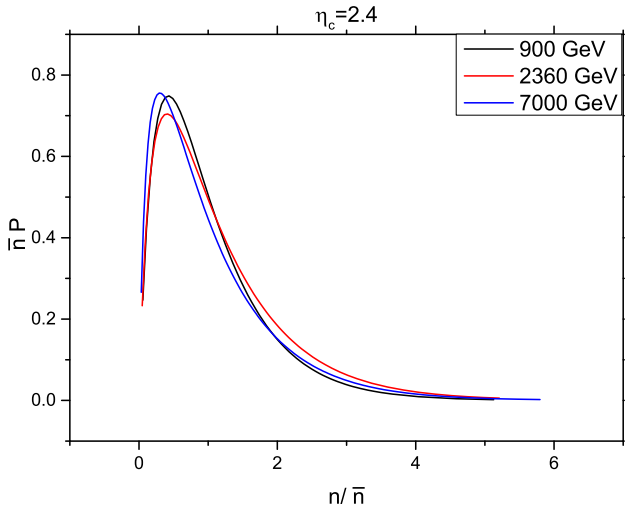

(b)

Figure 3.10: Shown are plots of $\Psi(z)$ against z for (a) $\eta_c = 0.5$ and (b) $\eta_c = 2.4$.

From figure 3.10, one can see that there is a obvious violation of KNO scaling at $\eta_c = 2.4$. However, at lower pseudorapidity ranges, $\eta_c = 0.5$ one can see that KNO scaling could still hold, i.e. the curves seem to align better at lower η_c.

The observation of KNO scaling violation at high η_c but not at low η_c leads one to infer that the scaling violation could be caused by particles with high pseudorapidity, i.e. the particles close to the beam axis and thus have low transverse momenta. In contrast, low η particles (high p_T) obey KNO-scaling implying that these two types of particles (high and low p_T) undergo different processes.

High p_T particles are of great interest since their momenta must come from the interaction process. Particles are accelerated along the beam axis, so almost all their momenta are along the beam axis. Thus, the high p_T of a particle must come from particle interactions, and not left over from the initial momentum along the beam axis.

Violation of KNO scaling at the low p_T region seems to indicate that this scaling scheme may be too simple. An extension or revision to this scheme is needed. The new scaling principle has to take into account the different processes of high and low η particles.

3.7 Discussion

An interesting point to note is that by obtaining an asymptotic solution of the QCD-parton branching equation, one obtains a probability distribution which can be used to model the multiplicity data. This solution takes into account two more processes than that of the GMD, and one notes that these two processes have non-zero branching probabilities ($B, C \neq 0$).

The trend in the fit parameters reflects the different behaviours of the branching processes in the jets. With data across a larger range of energies were available, one could then study this trend more precisely. The knowledge of how the fit parameters behave as a function energy would shed some light on how the different branching processes are affected with regard to energy. The relationship between the branching processes and energy could in turn provide a reason as to how hadronization occurs.

An important observation one makes from the results is that as the energy increases, so does the significance of gluon activity. At higher and higher energies, gluon activity is believed to be increasingly dominant. From the analysis above, higher energies seem to favour gluon production modes (increase of α and β, decrease of D). The increasing dominance of gluon activity is also reflected in the increase in k' over the decrease in k.

Although the model may seem to fit the data well, it is still unable to explain or reproduce the shouldering seen from the data. The shouldering structure is increasingly obvious at high η_c at higher energies. A revision of this model may be necessary to explain the shouldering structure.

Chapter 4

Predictions for LHC energies of $\sqrt{s} = 8, 13,$ and 14 TeV

A prediction of the behaviour of the multiplicity distribution for 8000, 13000 and 14000 GeV is made. To obtain such a prediction, one first has to extrapolate the fit parameters.

4.1 Extrapolation of Fit Parameters

A simple linear extrapolation for the fit parameters would not suffice. Figures 3.8a to 3.8c and 3.8e display this non-linear behaviour. However, a linear extrapolation can be done for parameter k.

The three parameters α, β and k' are extrapolated by making these few observations:

1. As Figure 3.8e shows, k' seems to increase exponentially with increasing energy.

2. The parameters α and β seem to depend logarithmically on the energy. (Figures 3.8a and 3.8b).

3. From Section 3.6, one makes the assumption that B decreases with energy; the behaviour of B can also be assumed to decay exponentially

with increasing energy. Since β is known to increase logarithmically (preceding point). The trend of D with increasing energy can be found.

The observations lead to extrapolation based on the following set of equations:

$$\alpha = a_1 + a_2 \ln(\sqrt{s})$$
$$\beta = a_3 + a_4 \ln(\sqrt{s})$$
$$D = \beta + B = a_3 + a_4 \ln(\sqrt{s}) + a_5 + a_6\, e^{-a_7\sqrt{s}}$$
$$k = a_8\, e^{a_9\sqrt{s}}$$
$$k' = a_{10} + a_{11}\sqrt{s}$$

Where a_i are constants determined from the fit parameters obtained from the data set studied. Here, the trend of B is modelled by the equation $B = a_5 + a_6\, e^{-a_7\sqrt{s}}$.

4.2 Predictions

Tables 4.1 to 4.6 summarize the predicted parameters as well as the predicted mean and moments of the multiplicity distribution at these three energies (8000, 13000 and 14000 GeV). Figure 4.1 displays the predicted multiplicity distributions graphically.

η_c	α	β	D	k	k'
0.5	1.71	1.90	2.20	6.04×10^{-03}	5.19×10^{-10}
1.0	2.39	2.54	2.93	3.56×10^{-03}	3.47×10^{-09}
1.5	2.74	2.93	3.41	2.95×10^{-03}	9.13×10^{-09}
2.0	2.96	3.20	3.81	8.42×10^{-04}	8.22×10^{-08}
2.4	3.11	3.37	3.97	2.86×10^{-05}	2.02×10^{-04}

Table 4.1: Predicted Fit Parameters for 8000 GeV

η_c	$\overline{n}$	C_2	C_3	C_4	C_5
0.5	7.29	1.69	3.97	11.67	40.07
1.0	14.04	1.68	3.84	10.85	35.66
1.5	20.72	1.65	3.67	9.99	31.57
2.0	27.61	1.62	3.50	9.05	26.73
2.4	32.44	1.61	3.41	8.59	24.38

Table 4.2: Predicted Mean and C_q moments for 8000 GeV

η_c	α	β	D	k	k'
0.5	1.93	2.03	2.32	5.93×10^{-04}	9.20×10^{-10}
1.0	2.69	2.70	3.08	1.28×10^{-04}	6.15×10^{-09}
1.5	3.04	3.09	3.57	8.16×10^{-05}	1.62×10^{-08}
2.0	3.26	3.36	3.97	8.10×10^{-06}	1.35×10^{-07}
2.4	3.41	3.54	4.13	1.80×10^{-08}	3.28×10^{-04}

Table 4.3: Predicted Fit Parameters for 13000 GeV

η_c	$\overline{n}$	C_2	C_3	C_4	C_5
0.5	8.25	1.67	3.84	10.82	35.30
1.0	16.14	1.64	3.63	9.72	30.27
1.5	23.76	1.61	3.45	8.91	26.78
2.0	31.40	1.58	3.25	7.93	21.99
2.4	36.67	1.57	3.16	7.45	19.63

Table 4.4: Predicted Mean and C_q moments for 13000 GeV

η_c	α	β	D	k	k'
0.5	2.99	2.05	2.33	3.73×10^{-04}	1.00×10^{-09}
1.0	4.13	2.73	3.11	6.59×10^{-05}	6.69×10^{-09}
1.5	4.50	3.11	3.60	3.98×10^{-05}	1.76×10^{-08}
2.0	4.73	3.39	4.00	3.20×10^{-06}	1.45×10^{-07}
2.4	4.90	3.56	4.16	4.12×10^{-09}	3.53×10^{-04}

Table 4.5: Predicted Fit Parameters for 14000 GeV

η_c	$\overline{n}$	C_2	C_3	C_4	C_5
0.5	8.40	1.67	3.81	10.68	34.58
1.0	16.45	1.64	3.59	9.57	29.56
1.5	24.21	1.61	3.41	8.77	26.16
2.0	31.97	1.57	3.21	7.78	21.37
2.4	37.32	1.56	3.12	7.29	19.01

Table 4.6: Predicted Mean and C_q moments for 14000 GeV

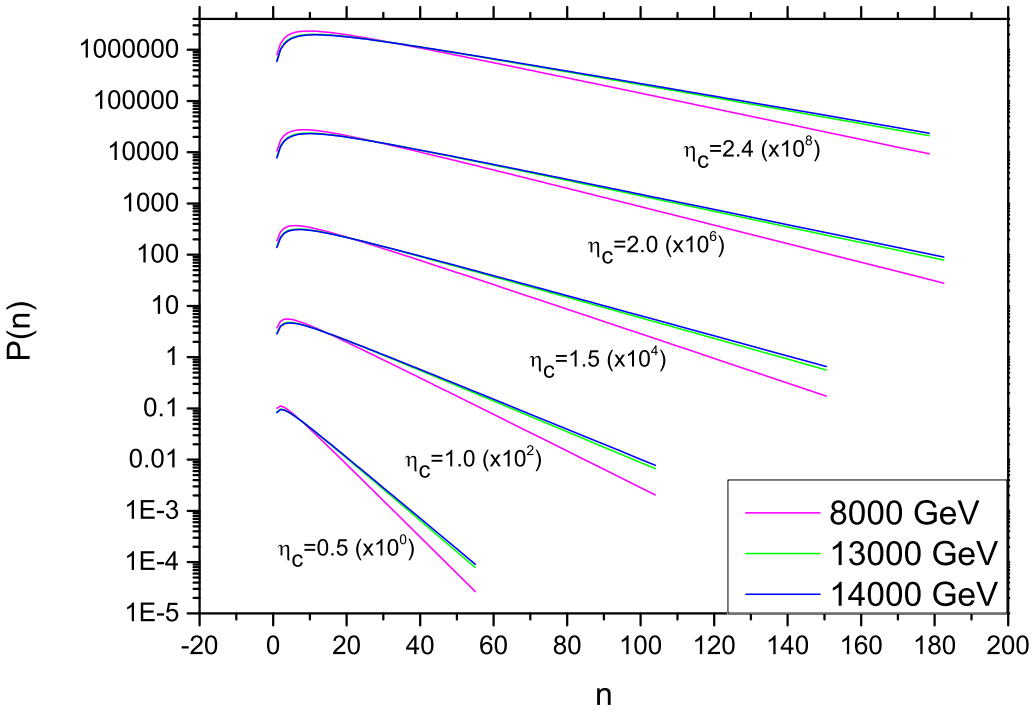

Figure 4.1: Predicted Curves for 8 TeV, 13 TeV and 14 TeV

With increasing energy, one predicts that the gluon activity will dominate quark activity. This is shown in the decrease in k with increasing energy and an increase in k' with increasing energy. The values for α and β as well as D are also predicted to increase as energy increases.

Since there is an increase in energy, the mean multiplicity is expected to increase as well.

One can deduce if there is KNO scaling violation from the C_q moments. From Tables 4.2, 4.4 and 4.6, the C_q moments for low η_c agree reasonably well across energies. At higher η_c the C_q moments do not agree as well. Thus, KNO scaling is predicted to hold at low η_c but violated at high η_c. Figure 4.2 display this prediction graphically.

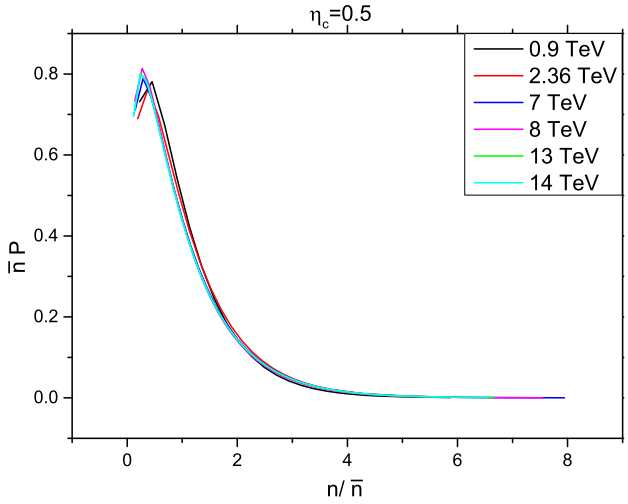

(a)

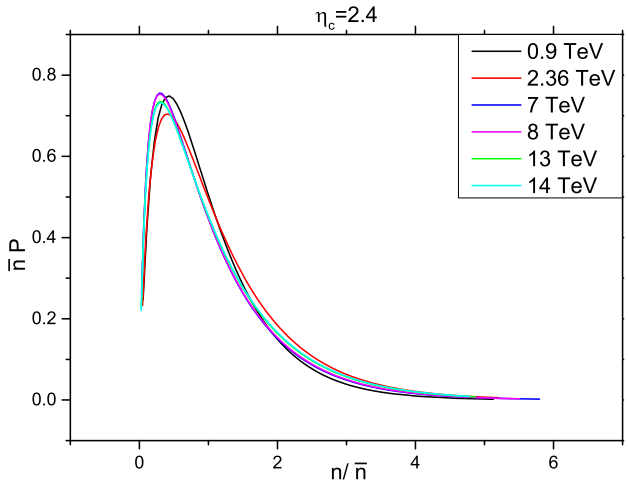

(b)

Figure 4.2: Shown are plots of $\Psi(z)$ against z for (a) $\eta_c = 0.5$ and (b) $\eta_c = 2.4$.

Chapter 5

Concluding Remarks

5.1 Conclusions

The motivation to shed light on the mechanism of hadronization led one to study the multiplicity distribution of pp collisions at various $\sqrt{s}$. This led to the derivation of the Asymptotic Solution to the QCD-Parton Branching Equation.

$$\begin{aligned} P(n) =& \frac{e^{-t(\alpha+(k'+1)\beta)}(1-e^{-\beta t})^{n-k'}}{\left[e^{-\beta t}(n-k') + \frac{D-\beta}{\beta}(1-e^{-\beta t})(1+k')\right]} \times (n-k') \\ & \times \frac{\Gamma(n+k+1)}{\Gamma(n-k'+1)\Gamma(k+k'+1)} \end{aligned} \tag{2.45}$$

The best-fitting Asymptotic Solution was then determined with experimental data and the parameters α, β, D, k and k' were obtained.

From the analysis of the fit parameters, one learns that as η_c increases:

1. α, β, D and k' increase for all $\sqrt{s}$.
2. k increases for $\sqrt{s} = 900$, 2360 GeV.
3. k decreases for $\sqrt{s} = 7000$ GeV.

leading to the conclusion that gluon branching increases with increasing η_c. Also, at higher energies, quark branching decreases (point 3).

One also learns from the comparison of the fit parameters across different $\sqrt{s}$ that:

1. α, β, and k' increases with increasing $\sqrt{s}$.
2. D and k decreases with increasing $\sqrt{s}$.

which implies that gluon branching dominates over quark branching at higher energies.

From the χ^2_{red} values, the asymptotic solution seems to be able to describe the data well, with all $\chi^2_{\text{red}} < 1$. However, the asymptotic solution is unable to reproduce the shouldering observed from the experimental data. KNO-scaling is also seen to be fulfilled at low η_c and violated at high η_c.

5.2 Future Work

Data from different experiments[23–27] from the LHC could be analysed as a consistency check. The parameters used above should agree at the same η_c. The significance difference in parameters would indicate that there are underlying issues that have yet to be understood.

With the LHC set to collect data at higher and higher energies, it would be interesting to see if the predictions made in the previous chapter would hold. Also, one is eager to find out if the shoulder-like structure becomes more prominent (or otherwise) at higher $\sqrt{s}$.

The presence of a shoulder structure seems to indicate that there could be more than one process involved. Thus one can consider a superposition of two processes:

$$P_n = \omega P_{\text{AS}}(\alpha_1, \beta_1, D_1, k_1, k_1') + (1-\omega) P_{\text{AS}}(\alpha_2, \beta_2, D_2, k_2, k_2') \tag{5.1}$$

where the subscript 1 and 2 refer to the processes involved, and ω is the superposition coefficient. Such superposition has been done for many distri-

butions[5,28] with the two processes being interpreted as soft and semi-hard processes[28]. At the increased energy, it would be interesting to see if this model would describe the data better as compared to other models. However, the flaw in the above method is that of number of parameters used.

Finally, an analytical solution for $\overline{n}$ is sought. If such a solution exist it could reduce the number of parameters used for the fitting process ($\overline{n}$ can be obtained experimentally).

Appendix A

Markov Branching Process

A Markov chain is a type of stochastic process in which the current state depends only on the immediately preceding state. If one deals with probabilities (as in the case for this study), one gets:

$$P(X_{n+1}|X_n, X_{n-1}, ..., X_0) = P(X_{n+1}|X_n) \tag{A.1}$$

where X_n represents a state X at time n.

Formally, for a Markov chain, the conditional distribution of any future state X_{n+1}, given past states $X_0, X_1, ..., X_{n-1}$, and present states X_n, is independent of all past states and only depends on the present state.

In a Markov branching process, each member of a population in some generation n produces a number 'offspring' in the subsequent generation $n + 1$ according to a fixed probability distribution.

A detailed explanation of the Markov branching processes can be found in [29].

Appendix B

Commonly Used Variables in Particle Physics

B.1 Pseudorapidity, η

B.1.1 Definition

Pseudorapidity is defined as:

$$\eta = -\ln\left[\tan\left(\frac{\theta}{2}\right)\right] \tag{B.1}$$

Figure B.1 below is a schematic representation of the collision point along the beam-axis. The beam-axis is denoted as the z-axis, while the y-axis is perpendicular to the plane of the paper. Thus, θ is the angle between the resultant particle momentum and the z-axis. Thus, with Eqn. (B.1), one can see that η ranges from $-\infty$ to $+\infty$, depending on the value of θ.

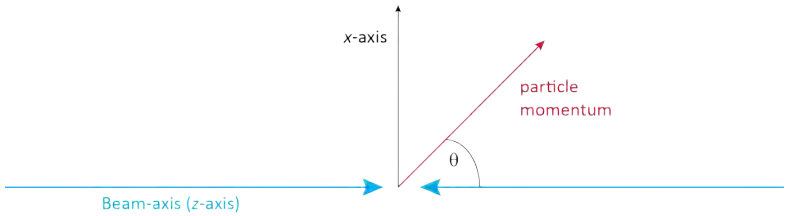

Figure B.1: Schematic Illustration for Pseudorapidity

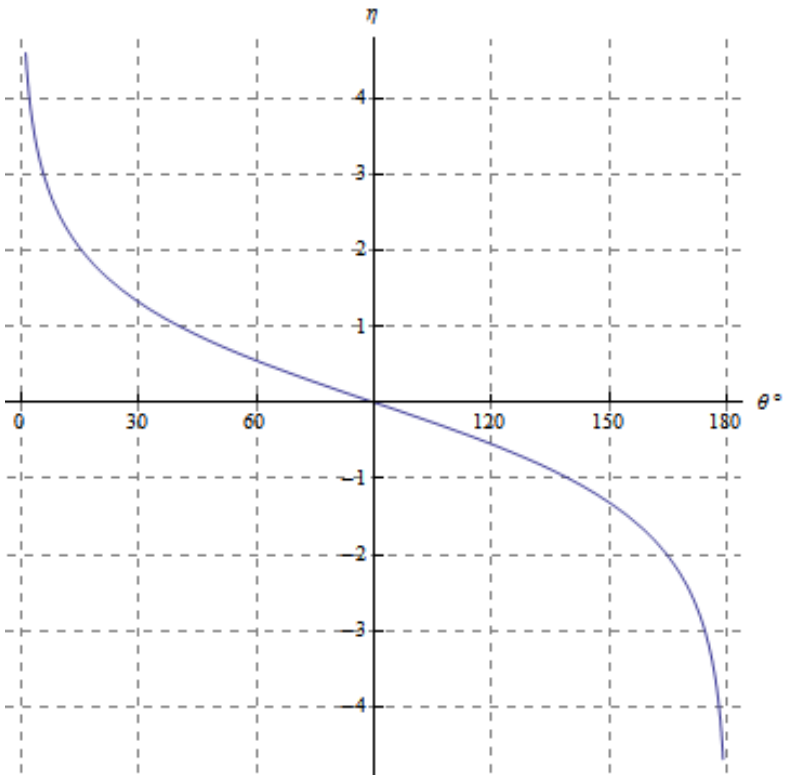

Figure B.2: Plot of Pseudorapidity η against polar angle θ.

B.1.2 Relation to Rapidity, y

Pseudorapidity can also be written in terms of the particle momentum $\vec{p}$.

$$\eta = \frac{1}{2} \ln \left(\frac{|\vec{p}| + p_{\mathrm{L}}}{|\vec{p}| - p_{\mathrm{L}}} \right) \tag{B.2}$$

The variable p_{L} here is the longitudinal momentum (momentum along the beam axis) of the particle.

This definition of η stems from the particle physics' definition of the rapidity, y:

$$y = \frac{1}{2} \ln \left(\frac{E + p_{\mathrm{L}}}{E - p_{\mathrm{L}}} \right) \tag{B.3}$$

For relativistic particles, $E \approx |\vec{p}|$, and thus

$$\eta \approx y \tag{B.4}$$

at high energies.

B.1.3 y vs η and their importance

These two quantities, rapidity and pseudorapidity, are useful in particle physics' because of their properties. It turns out that the difference in rapidity (and difference in pseudorapidity) are invariant quantities under a Lorentz boost in the z-axis.

$$y_1 - y_2 = y_1' - y_2'$$
$$\eta_1 - \eta_2 = \eta_1' - \eta_2'$$

It is common in hadron collisions that there is a leading quark or gluon with a higher momentum than the other particle. This causes the secondary particles (particles produced in collision) to be produced nearer one end of the beam axis. The Lorentz invariance enables the conversion of to the centre-of-mass frame of the leading quark without any loss of information.

Why then do particle physicists use pseudorapidity instead of rapidity? Pseudorapidity is a useful concept because it only depends on one variable, the polar angle θ. Thus, calculating pseudorapidity only requires an accurate measurement of the polar angle. In contrast, the calculation of rapidity would require us to know the particle mass (since we need both E and p). The measurement of particle mass is much more involved as compared to that of the polar angle. Also since modern colliders run at high energies, the two values are essentially the same. As such, pseudorapidity is more widely used as compared to rapidity.

B.2 Mandlestam Variables

Consider the scattering process $A+B \rightarrow C+D$. It is desirable to express the (scattering) amplitude as a function of Lorentz invariant variables. Particle physicists, by convention, use these set of variables known as the Mandelstam variables. The Mandelstam variables are defined as:

$$\begin{aligned} s &= (P_A + P_B)^2 = (P_C + P_D)^2 \\ t &= (P_A - P_C)^2 = (P_B - P_D)^2 \\ u &= (P_A - P_D)^2 = (P_B - P_C)^2 \end{aligned}$$

where P_i is the four-momentum of particle i. Here the Planck units are used ($c = 1$). The Feynman Diagrams in Figure B.3 depict examples of s-channel, t-channel, and u-channel processes.

Also, it can be shown that:

$$s + t + u = m_A^2 + m_B^2 + m_C^2 + m_D^2 \tag{B.5}$$

where m_i is the mass of particle i.

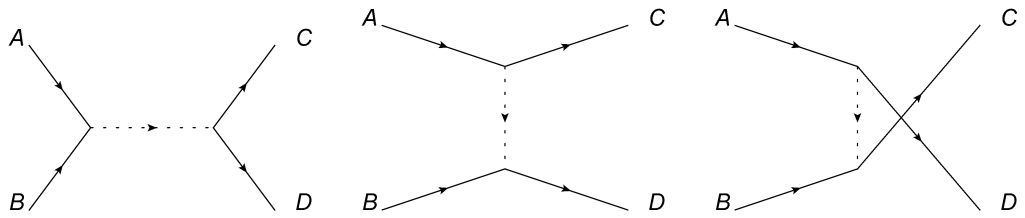

(a) s-channel (b) t-channel (c) u-channel

Figure B.3: Feynman Diagrams representing different scattering channels

B.2.1 More on $\sqrt{s}$

If we consider the center-of-mass frame, we have:

$$P_A = (E_A, \vec{p_A})$$
$$P_B = (E_B, -\vec{p}_A)$$

If we consider an s-channel process, then

$$\begin{aligned} s &= (E_A + E_B)^2 \\ s &= E_{\text{Tot}}^2 \\ \sqrt{s} &= E_{\text{Tot}} \end{aligned} \tag{B.6}$$

Thus we can see that $\sqrt{s}$ is just the total energy of the system.

Appendix C

Local Parton Hadron Duality

The theory of Local Parton-Hadron Duality (LPHD) posits that there is a direct correspondence (local) between partonic and hadronic spectra (duality) [30]. In other words, the **distributions of partons and hadrons are similar**. Experimental evidence for LPHD is shown in [31]. This theory has been applied to available data, but with many different interpretations (depending on the author). For instance, some follow literally the idea of "one parton - one hadron" equivalnce, while others believe that LPHD will work only if averages are taken (and not applied at an exclusive level) [32].

Appendix D

Feynman Scaling & KNO Scaling

D.1 Feynman Scaling

Feynman concluded that at asymptotically large energies,

$$\overline{n} \propto \ln \sqrt{s} \tag{2.50}$$

The relation above was obtained from phenomenological arguments about the exchange of quantum numbers between colliding particles. Feynman argued that the number of particles with a given mass and transverse momentum per longitudinal momentum interval p_z depends on energy $E = E(p_z)$ as

$$\frac{\mathrm{d}N}{\mathrm{d}p_z} \sim \frac{1}{E} \tag{D.1}$$

The probability of finding a particle of kind i with mass m and transverse and longitudinal momentum p_T and p_z is:

$$f_i(p_T, x_F)\frac{\mathrm{d}p_z}{E}\mathrm{d}^2p_T \tag{D.2}$$

with $E = \sqrt{m^2 + p_z^2 + p_T^2}$ and $x_F = 2p_z/\sqrt{s}$. The variable x_F is known as the *Feynman-x*. Feynman hypothesised that f_i becomes independent of $\sqrt{s}$

at high energies. The assumption is known as *Feynman scaling* with the function f_i known as the Feynman function or scaling function.

The relation given in Equation (2.50) is obtained by integrating Equation (D.2). A derivation can be found in [19].

D.2 KNO scaling

As mentioned in Section 2.4.1, KNO scaling is obtained by an extension of Feynman scaling. KNO scaling is derived by calculating:

$$\langle n(n-1)\dots(n-q+1)\rangle = \int f^{(q)}(p_{T,1}, x_1; \dots; p_{T,q}, x_q)\frac{\mathrm{d}p_{z,1}}{E_1}\mathrm{d}^2p_{T,1}\dots\frac{\mathrm{d}p_{z,q}}{E_q}\mathrm{d}^2p_{T,q} \tag{D.3}$$

Integration by parts is performed for all x_i, and with the substitution of the form $\overline{n} \propto \ln s$, the multiplicity distribution is found to scale as:

$$P(n) = \frac{1}{\overline{n}}\Psi(\frac{n}{\overline{n}}) + \mathcal{O}\left(\frac{1}{\overline{n}^2}\right) \tag{2.51}$$

The full derivation of KNO scaling can be found in [17].

References

[1] A. Cho, Science **337**, 141 (2012), http://www.sciencemag.org/content/337/6091/141.full.pdf, URL http://www.sciencemag.org/content/337/6091/141.short.

[2] B. R. Webber, International Journal of Modern Physics A **15**, 577 (2000).

[3] C. Chew and Y. Lim, Physics Letters B **163**, 257 (1985), ISSN 0370-2693, URL http://www.sciencedirect.com/science/article/pii/0370269385902333.

[4] I. Zborovskỳ, Journal of Physics G: Nuclear and Particle Physics **40**, 055005 (2013).

[5] A. Dewanto, A. Chan, and C. Oh, International Journal of Modern Physics E **16**, 3295 (2007).

[6] M. Biyajima and N. Suzuki, Physics Letters B **143**, 463 (1984), ISSN 0370-2693, URL http://www.sciencedirect.com/science/article/pii/037026938491503X.

[7] B. Durand and I. Sarcevic, Phys. Rev. D **36**, 2693 (1987), URL http://link.aps.org/doi/10.1103/PhysRevD.36.2693.

[8] I. Sarcevic, Phys. Rev. Lett. **59**, 403 (1987), URL http://link.aps.org/doi/10.1103/PhysRevLett.59.403.

[9] A. Chan and C. Chew, Physical Review D **41**, 851 (1990).

[10] S. Chatrchyan, V. Khachatryan, A. Sirunyan, A. Tumasyan, W. Adam, T. Bergauer, M. Dragicevic, J. Erö, C. Fabjan, M. Friedl, et al. (CMS), The European Physical Journal C **73**, 1 (2013).

[11] E. Kokoulina and A. Kutov, Physics of Atomic Nuclei **71**, 1543 (2008), ISSN 1063-7788, URL http://dx.doi.org/10.1134/S1063778808090081.

[12] E. Kokoulina, arXiv preprint hep-ph/0511111 (2005).

[13] T. Mizoguchi and M. Biyajima, The European Physical Journal C **70**, 1061 (2010), ISSN 1434-6044, URL http://dx.doi.org/10.1140/epjc/s10052-010-1505-1.

[14] A. Giovannini, Nuclear Physics B **161**, 429 (1979), ISSN 0550-3213, URL http://www.sciencedirect.com/science/article/pii/0550321379902220.

[15] A. H. Chan and C. K. Chew, Journal of Mathematical Physics **33**, 3209 (1992), URL http://link.aip.org/link/?JMP/33/3209/1.

[16] K. Riley, M. Hobson, and S. Bence, in *Mathematical Methods for Physics and Engineering (Third Edition)* (Cambridge University Press Press, 2006), p. 637, 3rd ed., ISBN 978-0-521-67971-8.

[17] Z. Koba, H. B. Nielsen, and P. Olesen, Nuclear Physics B **40**, 317 (1972).

[18] R. P. Feynman, Physical Review Letters **23**, 1415 (1969).

[19] J. F. Grosse-Oetringhaus and K. Reygers, Journal of Physics G: Nuclear and Particle Physics **37**, 083001 (2010).

[20] CMS Collaboration (CMS), Journal of High Energy Physics **2011**, 1 (2011), URL http://dx.doi.org/10.1007/JHEP01%282011%29079.

[21] The Durham HepData Project, *Khachatryan 2011 - Charged particle multiplicities in pp interactions at sqrt(s) = 0.9, 2.36, and 7 Tev* (2011), URL http://hepdata.cedar.ac.uk/view/irn8884919.

[22] S. J. Wright and J. Nocedal, in *Numerical Optimization* (Springer New York, 2006), Springer Series in Operations Research and Financial Engineering, pp. 245–269, ISBN 978-0-387-30303-1, URL http://dx.doi.org/10.1007/978-0-387-40065-5_10.

[23] G. Aad, B. Abbott, J. Abdallah, A. Abdelalim, A. Abdesselam, O. Abdinov, B. Abi, M. Abolins, H. Abramowicz, H. Abreu, et al. (ALTLAS), New Journal of Physics **13**, 053033 (2011).

[24] K. Aamodt, N. Abel, U. Abeysekara, A. A. Quintana, A. Abramyan, D. Adamova, M. Aggarwal, G. A. Rinella, A. Agocs, S. A. Salazar, et al. (ALICE), The European Physical Journal C **68**, 89 (2010).

[25] K. Aamodt, N. Abel, U. Abeysekara, A. A. Quintana, A. Abramyan, D. Adamova, M. Aggarwal, G. A. Rinella, A. Agocs, S. A. Salazar, et al. (ALICE), The European Physical Journal C **68**, 345 (2010).

[26] C. Zampolli et al. (ALICE), arXiv preprint arXiv:1310.7430 (2013).

[27] LHCb Collaboration (LHCb), The European Physical Journal C **72**, 1 (2012), ISSN 1434-6044, URL http://dx.doi.org/10.1140/epjc/s10052-012-1947-8.

[28] A. Giovannini and R. Ugoccioni, Physical Review D **59**, 094020 (1999).

[29] S. M. Ross, in *Introduction to Probability Models (Tenth Edition)* (Academic Press, Boston, 2010), pp. 191 – 290, 10th ed., ISBN 978-0-12-375686-2, URL http://www.sciencedirect.com/science/article/pii/B9780123756862000091.

[30] Y. I. Azimov, Y. L. Dokshitzer, V. A. Khoze, and S. Trovan, Zeitschrift für Physik C Particles and Fields **27**, 65 (1985).

[31] Y. I. Azimov, Y. L. Dokshitzer, V. A. Khoze, and S. Troyan, Zeitschrift für Physik C Particles and Fields **31**, 213 (1986).

[32] V. A. Khoze and W. Ochs, International Journal of Modern Physics A **12**, 2949 (1997).

[33] R. Vogt, in *Ultrarelativistic Heavy-Ion Collisions*, edited by R. Vogt (Elsevier Science B.V., Amsterdam, 2007), pp. 427 – 454, ISBN 978-0-444-52196-5, URL http://www.sciencedirect.com/science/article/pii/B9780444521965500098.

[34] W. Kittel and E. A. De Wolf, *Soft multihadron dynamics* (World Scientific, 2005).